University of California, Davis
Aeronautical and Environmental Wind Tunnel Facility
Department of Mechanical and Aeronautical Engineering
One Shields Avenue, Davis, California 95616-5294

FINAL REPORT

Contract No. 6503284

Existing Hillside and Proposed Building 75 Rooftop Stacks

A WIND-TUNNEL STUDY OF EXHAUST STACK EMISSIONS FROM THE NATIONAL TRITIUM LABELING FACILITY (NTLF) LOCATED AT LAWRANCE BERKELEY NATIONAL LABORATORY, BERKELEY, CA

Bruce R. White, Professor

Rachael Coquilla, Graduate Student

Jim Phoreman, Graduate Student

Prepared for:
Environmental, Health, & Safety Division
Ernest Orlando Lawrence Berkeley National Laboratory
University of California, Berkeley
Berkeley, California 94720

MAY 2001

TABLE OF CONTENTS

EXECUTIVE SUMMARY

A wind-tunnel study was conducted to simulate stack releases of tritiated water vapor (HTO) from its National Tritium Labeling Facility (NTLF). Physical modeling simulations were performed in the Atmospheric Boundary Layer Wind Tunnel (ABLWT) at University of California, Davis. A circular-based scaled-model (1:800) of the site represented a full-scale area of 3,000 feet (914 meters) in diameter, including all buildings, topography, and the relative tree cover. The model was also turntable mounted so that it could be rotated to any desired wind direction. Two stacks of different design and location were individually tested: i) an existing stack located in the same location as air sampling station ENV-75EG; and ii) a proposed stack to be built on the rooftop of Building 75. Stack effluent was modeled by releasing a neutrally buoyant tracer gas (ethane) from the scaled model exhaust system. Simultaneously, concentration (or dilution) levels of the dispersed emissions at specified downwind ground-level receptor sites were measured using a hydrocarbon gas analyzer. The wind tunnel simulated near-neutral atmospheric conditions (between stability category B and C of the Pasquill-Gifford categories). Tests were conducted over a wide range of wind regimes that dynamically matched full-scale speeds ranging from a few mph to speeds in excess of 25 mph.

Concentrations and dilution factors were measured over a uniform grid of 49 downwind test receptors for the two most frequent wind directions blowing from the west and southeast and for three common full-scale wind speeds: 2.5, 5, and 20 mph. Both the existing stack and the proposed stack on top of Building 75 were simulated. The downwind measurement area for both stack settings was approximately 600 by 600 feet in full scale. Based on the measured downwind dilutions from the west wind direction setting, the existing stack's performance proved slightly better than that of the proposed stack on Building 75. See Figure 15 to Figure 17 for the resulting concentration isolines for the existing stack and Figure 18 to Figure 20 for the results from proposed Building 75 stack. For the southeasterly wind direction, the result is opposite in which the proposed stack on top of Building 75 would provide better dilution in the comparable downwind areas than the existing stack. See Figure 21 to Figure 23 and Figure 24 to Figure 26 for the existing stack and the Building 75 stack results, respectively. These plots of concentration isolines would simulate routine exhaust releases for the common wind directions. The results also could be used to simulate an accidental release of non-elevated temperature effluent

resulting from non-scheduled event such as a large-magnitude earthquake, human error, major equipment failure, etc. An exposure estimate could be made by knowing (or assuming) the total amount of radiation release over a specified time and then by applying the dilution factors as a function of location. For example, if 0.1 Ci were released continuously for one hour and a downwind area measured a full-scale concentration of 10,000 ppm, which corresponds to a dilution factor of 10,000, the tritium radiation concentration would be $(0.1 \times 10^{12}$ pCi)(100 PPM/10^6)(1 hr/11,044 m^3) = 905.47 pCi/m^3. This is approximately the amount of tritium radiation processed during one day's operation for an annual release rate of 30 Ci HTO per year. Other scenarios also may be easily calculated using the same technique.

Wind-tunnel tests also were conducted to determine the annual averaged tritium concentration in pCi/m^3 for yearly releases of 30 and 100 Ci HTO respectively. It was assumed that the release process operated 24 hours per day and seven days per week during an entire year. The wind-tunnel results are displayed in Figure 27 to Figure 30. The red circular dotted line represents the physical size of the area simulated on the turntables during the testing. Figure 31 and Figure 32 display the SENES Oak Ridge Inc. CALPUFF predictions of tritium concentration (pCi/m^3) for the same set of isoline contours based on the identical yearly releases of 30 and 100 Ci HTO, respectively. Patterns of dispersion predicted by the two approaches (CALPUFF and wind tunnel) differ slightly; however, the magnitudes of concentrations estimated by each approach are similar.

INTRODUCTION

This report documents a wind-tunnel study of the release of tritiated water vapor (HTO) from existing and proposed exhaust stacks located at the National Tritium Labeling Facility (NTLF) of the Ernest Orlando Lawrence Berkeley National Laboratory. The study was primarily driven by the interest of where to appropriately locate proposed air monitoring stations. Results from this study would provide physical modeling information for positioning proposed tritium monitoring stations. The existing stack is 9.14 m (30 ft) tall and 1 m (3.28 ft) in diameter (see Figure 1). It is solely situated on the hillside slope of the Eucalyptus Grove above and to the west of NTLF Building 75 and is surrounded by numerous tall Eucalyptus trees. The proposed stack is to be constructed on the rooftop of Building 75 with a height of 4.57 m (15 ft) and a square exit cross-section of 20 by 20 inches. Both stacks are also bordered by steep topographic inclines spanning from west to east. A photo consisting of the existing stack and the location of the proposed stack is presented in Figure 2. The main objectives of the current investigation is to assess the nature of the local flow effects due to the complex terrain features of the Berkeley hills and to estimate the magnitude of concentrations dispersed from the source stacks.

Figure 1: Site photo of existing stack located inside Eucalyptus Grove hillside.

Figure 2: Site photo of existing stack and proposed location of Building 75 stack.

Comparison of Atmospheric Modeling Techniques

Dispersion of potentially hazardous stack exhausts is of great concern when addressing the possible consequences of such releases on human health and safety and on the environment

near the stack. Many variables affect the dispersion of exhausts from a stack such as wind speed and direction; stability of the atmosphere; stack height; surrounding buildings, trees, and topography; stack exhaust velocity; and initial pollutant concentrations.

Environmental assessment of an exhaust stack can be approached in three different techniques: numerical modeling, full-scale tests, or wind-tunnel simulation. Numerical models, dispersion models in particular, incorporate semi-empirical theory that generally leads to reasonable predictions of concentration levels around and even beyond the vicinity of the source emission. Many numerical models are also limited by failing to account for the local effects of nearby obstacles and of complex topography or by requiring locally measured turbulence data. Full-scale dispersion tests provide useful data for determining true concentration levels. However, conducting full-scale tests for numerous wind directions and wind speeds is relatively impractical.

Physical modeling in a wind tunnel has great potential for the simulation of atmospheric boundary layers. A model of the site of interest is placed in a wind tunnel where wind-speed and dispersion measurements can be taken. This modeling technique can be an efficient means of obtaining reasonable estimates of a desired data while properly accounting for local flow around obstacles and turbulence characteristics of the full-scale flows.

Wind tunnel testing could also be utilized for physically simulating the flow field over highly complicated terrain conditions such as the hills around the Lawrence Berkeley National Laboratory. For terrain with complex topography, where the height changes in the order of the height of the release stack, both physical and/or numerical simulation techniques required the input of additional field measurements, especially meteorological measurements on the site. On-site wind speed, wind frequency, and atmospheric stability measurements are very important for the accurate simulation whether it is numerical or physical in nature. However, the ability of physical modeling to simulate the turbulence characteristics of the flow over small-scale terrain features in nearly neutral flow is still considered superior to available numerical models. Therefore, physical modeling can be helpful in the process of evaluating the dispersion process from a source stack. The only drawback is that the wind tunnel used in the current investigation did not simulate non-neutral atmospheric conditions that can add substantial effects on the nature of the dispersion process.

Wind-Tunnel Atmospheric Modeling Parameters Emphasizing Complex Terrain

The present wind-tunnel investigation was performed in the Atmospheric Boundary Layer Wind Tunnel (ABLWT) located at University of California, Davis (UCD). A detailed description of the facility is given in Appendix A. Testing was conducted using a 1:800-inch scaled-model built on a 1.15-m diameter turntable base and centered on the site of the existing exhaust stack. Figure 3 presents a photo of the model installed inside the wind tunnel test section. In full scale, the model would encompasses an area with a diameter of 3,000, which includes not only buildings of the national laboratory but also the Lawrence Hall of Science, the Math Sciences Research Institute, and the Space Science facilities, as well as all tree groves contained within the area. A small model scale was chosen due to the complexity of the terrain.

Figure 3: Wind tunnel scaled model of the Berkeley hills
with the Lawrence Berkeley National Laboratory.

Since models used in a wind-tunnel simulation are typically orders of magnitude smaller than the full-scale object, it is not obvious that the results obtained will be corresponding to nature. However, results from wind-tunnel tests can be representative to full-scale conditions, as long as critical simulation of flow parameters between the model and full-scale are satisfied. For exact modeling, all flow parameters should be matched, which is impracticable, if not impossible. Thus, similitude parameters, critical to the modeling of the present wind-tunnel simulation, must be selected.

By normalizing the time-averaged equations of fluid motion, similitude parameters are given by the Rossby number, the Densimetric Froude number, the Prandtl number, the Eckert number, and the Reynolds number. Application of these non-dimensional quantities along with

their host equations of motion can describe atmospheric flows over all types of terrain conditions, including those that are complex in nature. Based on an analysis of the similitude parameters presented in Appendix C, only the critical Reynolds numbers related to boundary-layer dynamic similarity are important for the current wind tunnel modeling (given that the targeted simulated flow is neutrally stable and corresponds only to the lowest hundred meters of the atmosphere). Thus, for the current investigation, the Rossby number similarity is neglected since effects of upper atmospheric motion, driven by the earth's rotation, become insignificant for length scales less than five miles. Froude number matching is ignored for neutrally stable conditions. The Prandtl number already matches since the fluid media is identically air. The Eckert number is excluded since the modeled and full-scale flows are incompressible.

Wind-Tunnel Atmospheric Boundary Layer Similarity For Complex Terrain

Physical modeling of the complex terrain was additionally limited by the required atmospheric boundary-layer similarities and by the physical size constraints of the wind-tunnel test section. Analysis of such modeling conditions is presented in Appendix D. A circular turntable model can easily encompass the entire 1.18-m width of the test section. However, geometric scaling was restricted given two critical conditions: i) the highest point on the model is maintained within the wind tunnel boundary layer region that meets full-scale similarity; and ii) the model cross-sectional area facing the incoming flow does not cover more than 15% of the test section cross-section so as to prevent pressure-gradient driven flow.

Boundary-layer similarities were satisfied by the long flow development design of the Atmospheric Boundary Layer Wind Tunnel. With the use of triangular spires and the distribution of roughness elements, a fully developed aerodynamically rough boundary layer is generated at the test section. For a free stream wind tunnel speed of 3.8 to 4.0 m/s, the boundary layer grows to a height of about one meter at the test section, in which the logarithmic wind profile region is in the lowest 20%. Since this region is the only portion of the wind-tunnel boundary layer that is dynamic similar to the surface region of the atmosphere, the first requirement suggested that the model be scaled so that the highest peak of the terrain is no higher than 0.2 m. If the model diameter was equivalent to the test section width, a 0.2-m height limitation provides a model cross-sectional area much less than 15% of the test section cross-section.

Since the main objective of the wind-tunnel study was to trace the resulting concentration distribution due to the effects of complex topography, a model representing the largest full-scale area that essentially includes the most dominant terrain features was initially considered. Thus, the turntable model was constructed on a 1.15-m diameter base, spanning the test-section width. Considering the size and similarity constraints, the wind tunnel model was geometrically sized using a 1:800-inch reduction. Centering on the UC grid coordinates, 3500E and 500N, which is near the location of the existing stack, the wind tunnel model depicted a circular full-scale area 3000 ft. in diameter. Although, the wind tunnel model can represents only a few kilometers of the regional topography, it still captures the most distinct land features that could contribute significant local dispersion process of stack emissions. Wind-tunnel simulation can be a useful tool in the analysis of the dispersion process within a complex terrain region such as the hills around the Lawrence Berkeley National Laboratory.

Wind-Tunnel Stack Emission Dispersion Modeling

Stack emissions were modeled using a neutrally buoyant, hydrocarbon tracer gas. By monitoring hydrocarbon concentration levels with an ion flame detection system, the dilution of the stack emissions was determined at a measured receptor location. The scaling was accomplished by maintaining the momentum ratio of the vertical exhaust effluent to the horizontal wind speed, at the stack height and location, constant between full scale and the wind-tunnel simulation. To insure a fully turbulent discharge, a tripping device was incorporated in to the model exhaust stack. The full-scale meteorological data, acquired on 20-meter tower near Building 44, used in the following manner to determine the wind speed at which the model test was to be conducted. The wind speed and direction, in the tunnel, was set to model the full-scale conditions at the meteorological tower, the wind speed then was measured in the wind tunnel at the model stack location and height. Note, this value could be substantially different from the speed observed at the metrological tower due to the affect on the complex terrain on the wind flow patterns. Thus, it was essential to correlate the relationship between the metrological tower speed and direction to that of the speed and direction the wind at the top of the stack being measured. This correlation data was measured for all 16 major wind sectors used in the annual average analysis and the wind-tunnel settings made according to the results of the correlation.

WIND TUNNEL RESULTS AND ANALYSIS

Wind tunnel simulations were divided into three test phases. An initial test was performed to examine the horizontal dispersion of the exhaust plume downwind of the source stack. In the second phase, concentrations were collected over a grid network of 49 points around the emission source, representing a 600-ft by 600-ft square area. For the third phase, measurements over a larger grid system that encompassed the entire wind-tunnel turntable model were conducted for estimation of annual average exposure levels.

Phase 1: Effect of Complex Terrain on the Dispersion of Stack Emissions

In the first phase of wind tunnel simulations, the downwind dispersion of emissions from the existing stack model was traced to determine the combined effects of angular wind offset and of the surrounding complex terrain. Wind speeds at the stack height were simulated based on equivalent full-scale magnitudes of 2.5, 5, and 20 mph. According to atmospheric field data recorded from a nearby 20-m meteorological (MET) tower located at LBNL Building 44 (see Table 1), local wind speeds routinely range from 0.5 to 20 mph.

Table 1: Wind data obtained from August 1, 1998 to July 31, 1999 at the Lawrence Berkeley National Laboratory 20-m meteorological tower located at Building 44

Wind Direction	Hours of occurrence per wind speed bin						Total hours per wind direction
	1-3 knots	4-6 knots	7-10 knots	11-16 knots	17-21 knots	>21 knots	
N	35	56	80	43	20	2	236
NNE	32	58	27	8	0	0	125
NE	26	36	27	7	0	0	96
ENE	33	47	42	50	25	26	223
E	59	105	88	74	31	55	412
ESE	73	200	197	171	54	23	718
SE	***88***	***263***	***315***	***255***	***115***	***86***	***1122***
SSE	61	198	229	92	20	10	610
S	41	149	176	59	10	5	440
SSW	39	117	149	26	3	1	335
SW	35	143	187	29	4	1	399
WSW	38	201	333	156	7	0	735
W	***77***	***302***	***475***	***364***	***31***	***0***	***1249***
WNW	87	280	401	193	34	11	1006
NW	105	196	162	118	17	1	599
NNW	59	115	114	116	41	4	449
Total hours per bin	888	2466	3002	1761	412	225	*8754* ** *Total Hours*

** Inconsistency of value for total hours to the total number of 8760 hours in a year is due to rounding errors.

Single-source emission dispersion over flat terrain is Gaussian in nature where the highest downwind concentrations are expected to fall at locations directly centerline from the stack. Due to the complex terrain in which the national laboratory is situated, exhaust dispersions may not always be Gaussian where the downwind peak concentrations could be off centerline from the direction of the incoming wind angle. Described in Table 2 and located on the map in Figure 4 are four test point locations found to be useful for examining concentration measurement sensitivity.

Table 2: Coordinate locations of test points for Phase 1 wind-tunnel simulation.

Test Point #	UC Grid Lateral Coordinate (ft)	UC Grid Longitudinal Coordinate (ft)	Location Description
1	3465 E	875 N	Site of ENV-LHS air sampling station
8	3475 E	1350 N	North parking lot of Lawrence Hall of Science
18	3400 E	1875 N	Buildings located south of Summit Road
20	3527 E	566 N	Site of ENV-75EG air sampling station

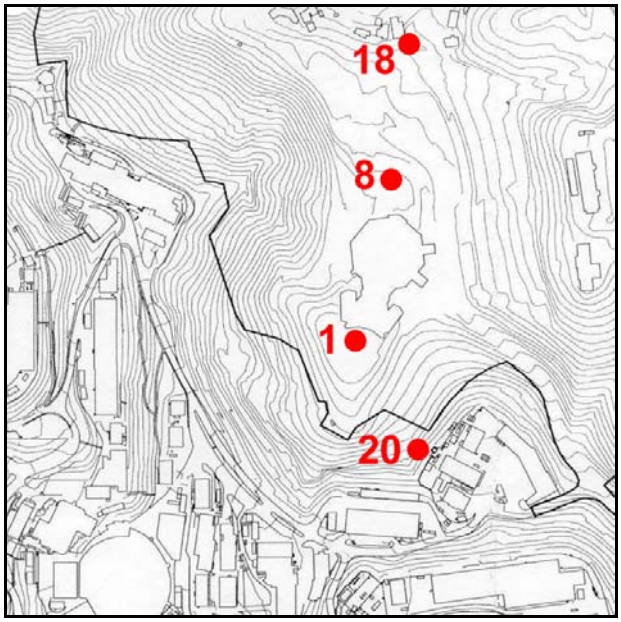

Figure 4: Map locations of Phase 1 test points.

Downwind concentration measurements for each wind-speed model were first attempted for a setting where the test points were at a straight-line distance directly downwind from the source stack. Such a baseline setting was referred to as the "zero-angle". Using the same wind speed range, measurements were then made at the same test point location for a range of angle rotations clockwise and counter-clockwise about the source stack (as viewed from above) deviating the test location away from the "zero angle" setting. The angular offset was continually increased in both rotational directions about the "zero angle" until the concentration measurements were no longer sensitive to angular variation or negligible in magnitude.

Resulting graphs of full-scale concentrations and dilution factors measured at each of the Phase 1 test point locations are presented in Figure 5 to Figure 8 and Figure 9 to Figure 12, respectively, for a range of simulated wind speeds at the height of the stack. Accordingly, an observed trend was that the highest concentrations were measured for settings where the test point location was directly downwind from the stack (i.e. zero angle) and also for stack wind-speeds corresponding to 2.5 mph or less in full-scale. The exception was point #20, located at the UC grid system coordinates, 3527 E and 566 N, the immediate vicinity of the Eucalyptus Grove air-monitoring station location (ENV-75EG). For a simulated 2.5 mph full-scale wind, a maximum concentration of 12,063 PPM was predicted when point #20 was rotated from the "zero angle" setting at an angle of –20°.

This initial test simulation produced concentration measurements within the same major wind sector (i.e. south, southwest, etc.). Thus, the data would not appropriate for calculation of annual average concentrations, which incorporate MET tower data for all wind directions impinging upon any given point. However, a particularly important deduction from this phase showed that the nature of the complex terrain would contain the downwind exhaust plumes within a maximum ±22.5° angular dispersion.

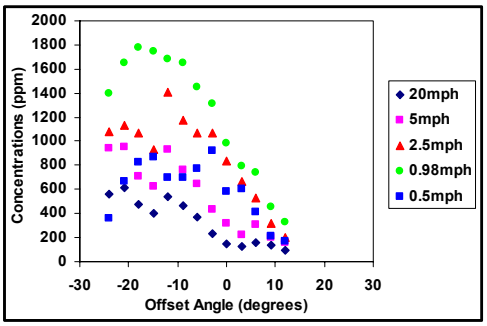

Figure 5: Full-scale concentrations at Point #1 at each rotation from the dispersion centerline.

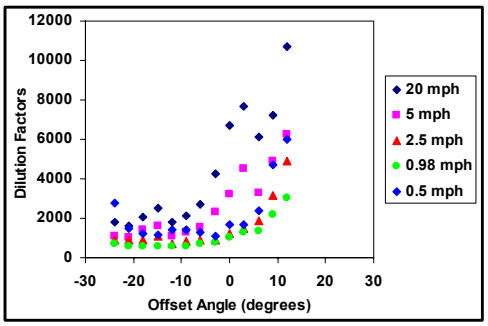

Figure 9: Dilution factors at Point #1 at each rotation from the dispersion centerline.

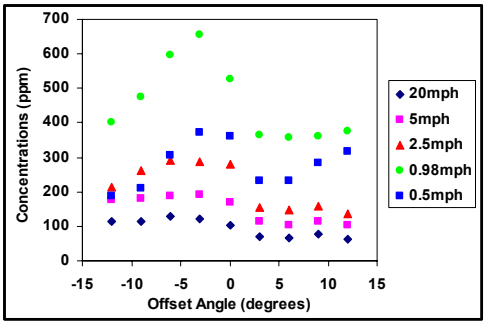

Figure 6: Full-scale concentrations at Point #8 at each rotation from the dispersion centerline.

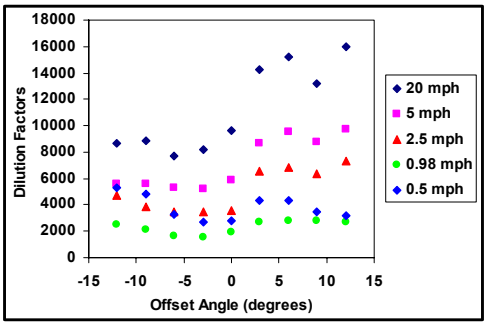

Figure 10: Dilution factors at Point #8 at each rotation from the dispersion centerline.

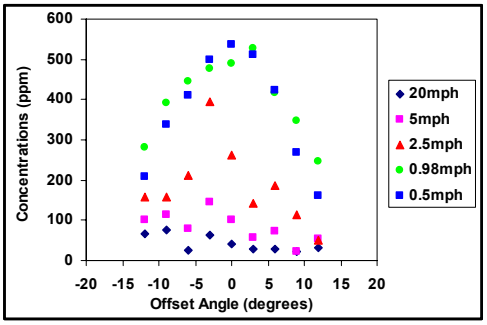

Figure 7: Full-scale concentrations at Point #18 at each rotation from the dispersion centerline.

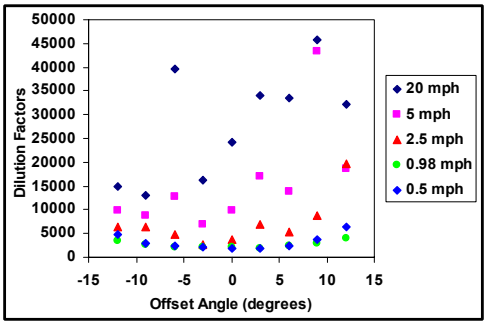

Figure 11: Dilution factors at Point #18 at each rotation from the dispersion centerline.

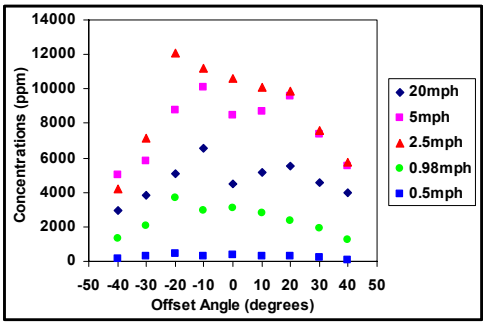

Figure 8: Full-scale concentrations at Point #20 at each rotation from the dispersion centerline.

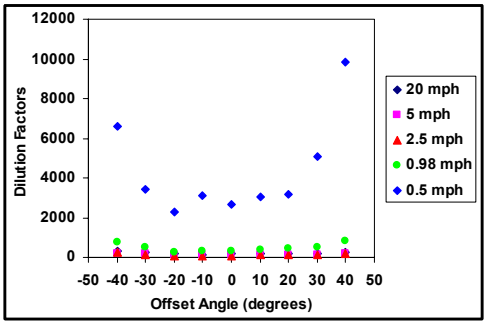

Figure 12: Dilution factors at Point #20 at each rotation from the dispersion centerline.

Phase 2: Contours for Two Predominant Wind Directions

The objective of second phase of wind-tunnel simulations was to collect concentration samples over a grid network of 49 points around the emission source, representing a 600-ft by 600-ft square area, for releases dispersed from the existing stack and from the proposed stack on the roof of Building 75. Similar to Phase 1, the range of commonly occurring winds at LBNL was modeled correspondingly to 2.5, 5, and 20 mph in full-scale at the stack height. Winds originating from the Southeast and West were also simulated since these were the two most frequent wind directions (see Table 1).

Each grid network was sampled for the three wind speeds and two directions with its upwind edge centered on the original stack location at UC grid coordinates, 3550 E and 520 N. The grid was later shifted to center the upwind edge on the proposed Building 75 stack location at UC grid coordinates, 3622 E and 449 N. Figure 13 is the grid sampled for the wind from West. Figure 14 is the grid sampled for the wind from Southeast.

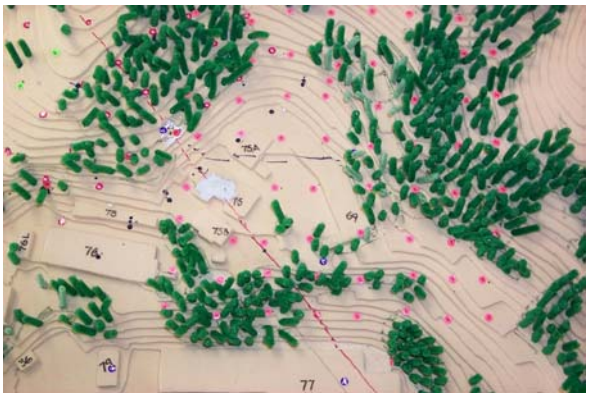

Figure 13: Phase 2 grid network of test locations for west wind setting.

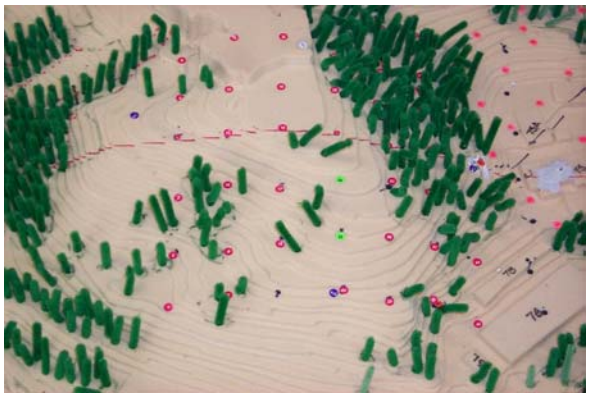

Figure 14: Phase 2 grid network of test locations for southeast wind setting.

In all, twelve contour plots were produced and are presented in Figure 15 thru Figure 26. Figure 15 to Figure 17 present concentration contours for the original stack with winds originating from the West, blowing directly toward Building 69. Examination of these contours will show the 20-mph wind from the West to have a highest peak concentration of 11,000 ppm located near the stack. This trend was a common observation for higher wind speeds simulated over the stack. It is a result of the effluent being pulled into the stack wake. This is commonly referred to as a downwash effect, prevalent at high wind speeds. Another observation is the second peak seen in each of these plots. This peak occurs near the vicinity of Building 69 and is evidently caused by the plume trajectory impacting onto the hill located directly to the East

(relative to grid North) as the plume impinges on this elevated terrain. The values of this second peak were as low as 120 ppm for the more dispersive 20-mph wind and as high as 480 PPM for the lower wind case of 2.5 mph.

Figure 18 to Figure 20 present concentration contours generated by a west wind for the proposed 15-ft stack at Building 75. This stack has a cross-sectional area of 400 in^2 and a volumetric flow rate of 6500 cfm. Thus, the exit velocity is 39 ft/s compared to 14.7 ft/s for the original stack. This higher exit velocity explains the absence of a peak concentration value near the base of the stack for the 2.5 and 5.0 mph wind speed cases since the effluent has more momentum to escape the downwind stack wake. The peak concentrations range from 490 ppm in the 5-mph case to 770 ppm in the 2.5-mph case and occur near the vicinity of Building 69. The 20-mph case exhibits a high wind behavior similar to the downwash flow observed from the existing stack simulation where the effluent is pulled into the wake of the stack. This wind condition resulted to a 1500-ppm peak concentration near the base. A second peak concentration as high as 200 ppm was also observed again at the site of Building 69. The irregular contour shape is due to the large-scale circulation of the flow field and the mixing associated with this occurrence because of the higher wind speeds and complex terrain.

Figure 21 to Figure 23 display concentration contours for the existing stack for winds blowing from the Southeast, generally towards the Lawrence Hall of Science. These plots show similar concentration contours with maximum concentrations of approximately 5000 ppm occurring within a 140-ft radius of UC grid coordinates 3400 E and 600 N. The concentration values decline rapidly in the Northeast and Southwest directions. The 20-mph wind speed case in Figure 23 shows the peak concentration of 7200 ppm localized in the immediate vicinity of the stack. The concentration falls to 1000 ppm within 300 feet of the stack in the downwind direction.

Figure 24 to Figure 26 present concentration contours for the Building 75 stack for the Southeast wind direction. These concentrations are generally lower than those measured for the existing stack location due to a relatively lower volumetric flow rate of 6500 cfm coupled with its 39 ft/s exit velocity. The combined effects of these two factors facilitate faster mixing rates and dilution of the plume. Figure 24 shows the effect of decreased plume mixing due to the relatively lower 2.5-mph wind. The contours show a plume with a concentration of 1400 ppm extending approximately 560 feet in the downwind direction. The 5 and 20 mph wind cases,

shown by Figures 14 and 15, respectively, demonstrate that the Building 75 stack would have relatively lower concentration values than the original stack location for this same direction.

The twelve contour plots from this test phase illustrate results that would lend well to the study of a worst case, accidental release scenario. These results are for constant wind directions and are only appropriate for the examination of events occurring on a time scale less than, approximately, one hour. The following example illustrates a means for calculating exposures in the scenario mentioned above.

$$\text{Total Exposure} = \text{Amount of Ci released} * \frac{1}{\text{Dilution Factor}} * \frac{1}{\text{Total Volumetric Flowrate}}$$

Dimensionally, the formula is the following:

$$\text{Total Exposure}\left[\text{pCi}/\text{m}^3\right] = \left(\text{X}\left[\text{Ci}\right]\right) * \left(\frac{10^{12}\left[\text{pCi}\right]}{1\left[\text{Ci}\right]}\right) * \left(\frac{\text{C}\left[\text{ppm}\right]}{10^6}\right) * \left(\frac{1\left[\text{hr}\right]}{1\left[\text{m}^3\right]}\right)$$

Here, 'X' is the total amount of concentration in Ci released in one hour, 'C' is the concentration from the desired location on the contour plots, and m^3 is the total volumetric flow rate of the mixture released in the units of cubic meters per hour. Entering the following example values for an accidental release scenario:

X = 1 Ci

C = 100 ppm (at a fictitious point location selected form a contour plot)

Flow rate = (6500 CFM)(0.3048 m/ft)^3(60 min/hr) = 11,044 m^3/hr

The resulting exposure is calculated to be:

Exposure = (1 x 10^{12} pCi)(100 ppm/10^6)(1 hr/11,044 m^3) = 9054.7 pCi/m^3.

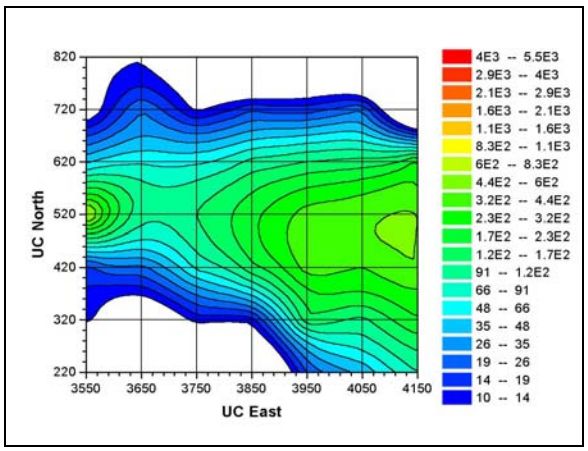

Figure 15: Concentration isolines (PPM) measured from the existing stack for a 2.5 mph westerly wind.

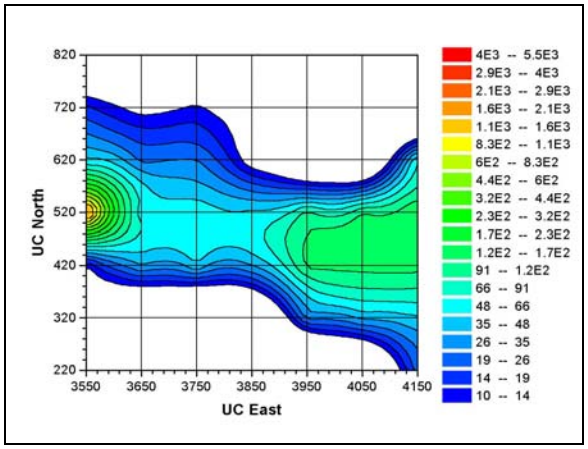

Figure 16: Concentration isolines (PPM) measured from the existing stack for 5 mph westerly wind.

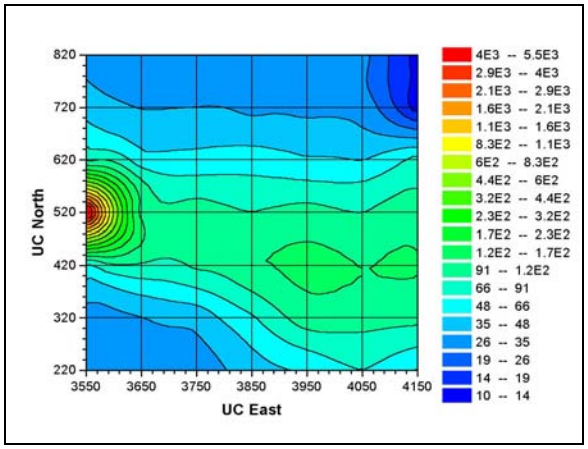

Figure 17: Concentration isolines (PPM) measured from the existing stack for a 20 mph westerly wind.

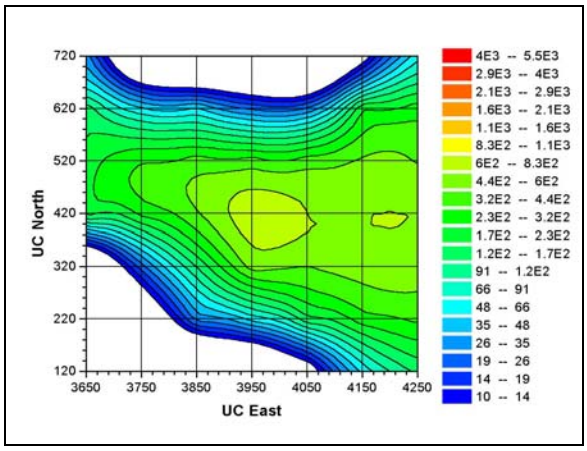

Figure 18: Concentration isolines (PPM) measured from the proposed Building 75 stack for a 2.5 mph westerly wind.

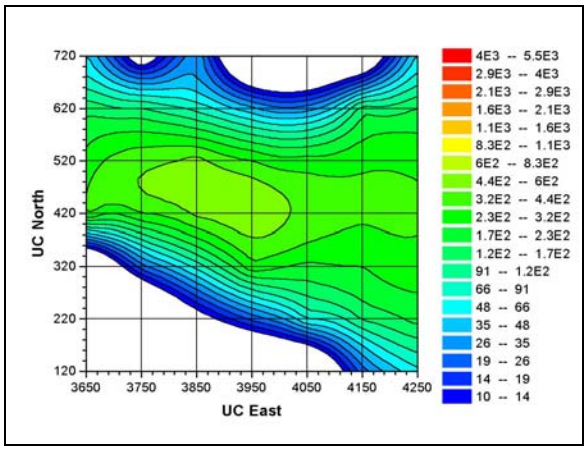

Figure 19: Concentration isolines (PPM) measured from the proposed Building 75 stack for a 5 mph westerly wind.

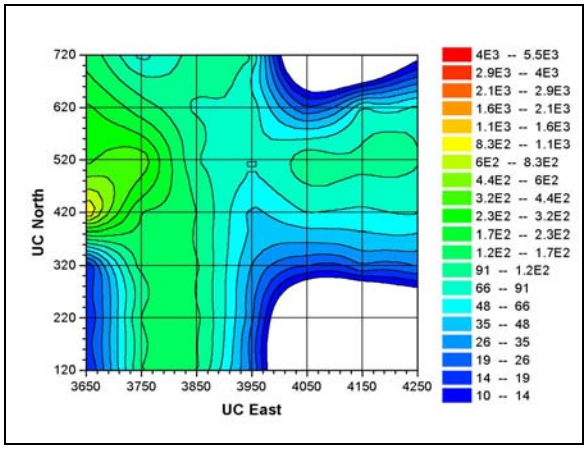

Figure 20: Concentration isolines (PPM) measured from the proposed Building 75 stack for a 20 mph westerly wind.

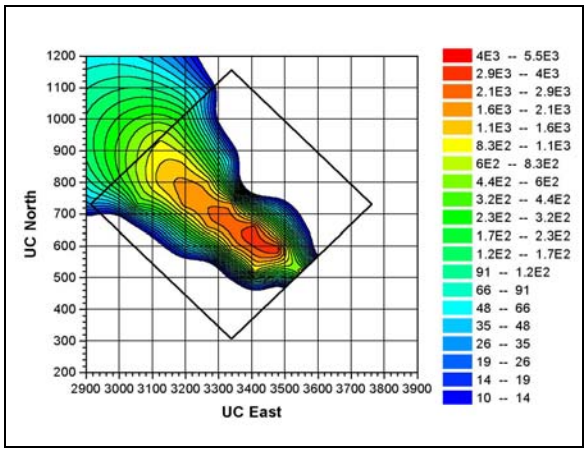

Figure 21: Concentration isolines (PPM) measured from the existing stack for a 2.5 mph southwesterly wind.

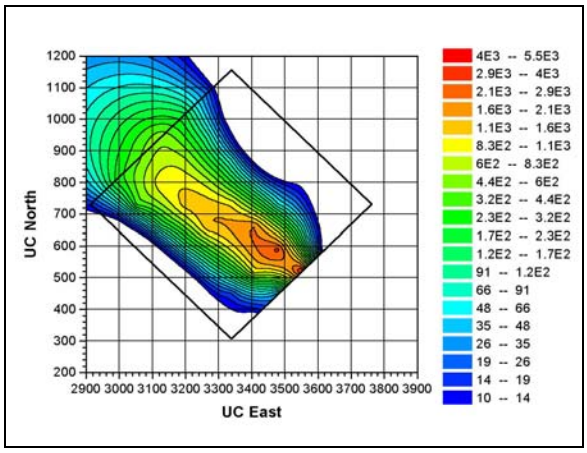

Figure 22: Concentration isolines (PPM) measured from the existing stack for a 5 mph southwesterly wind.

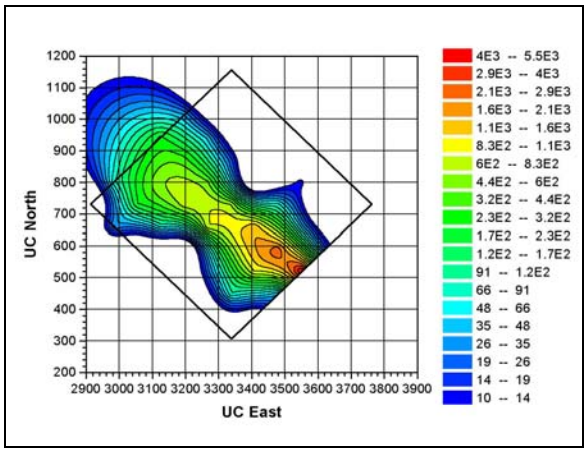

Figure 23: Concentration isolines (PPM) measured from the existing stack for a 20 mph southwesterly wind.

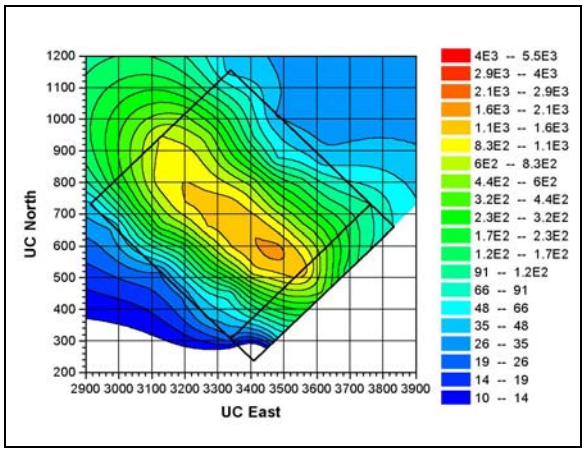

Figure 24: Concentration isolines (PPM) measured from the proposed Building 75 stack for a 2.5 mph southwesterly wind.

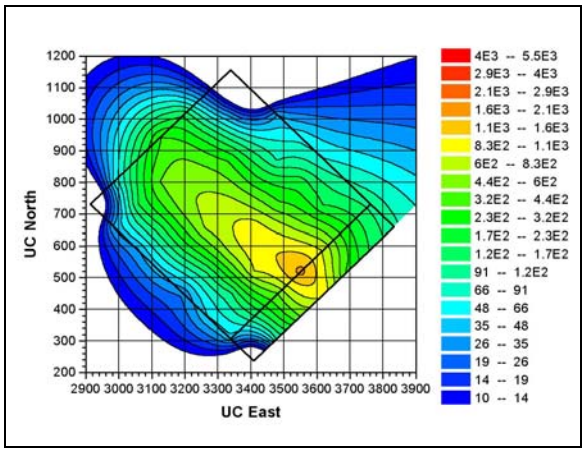

Figure 25: Concentration isolines (PPM) measured from the proposed Building 75 stack for a 5 mph southwesterly wind.

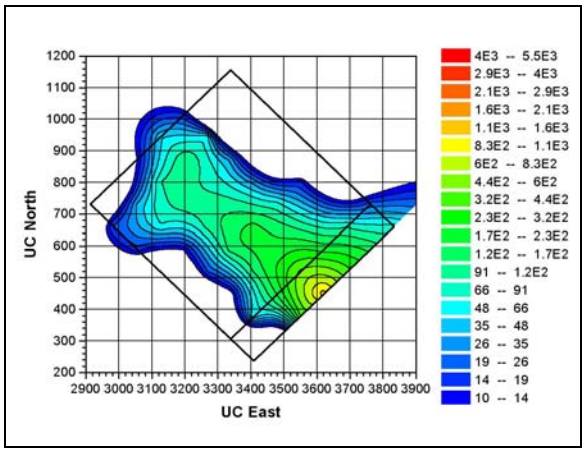

Figure 26: Concentration isolines (PPM) measured from the proposed Building 75 stack for a 20 mph southwesterly wind.

Phase 3: Concentration Distributions For a Given Annual Release

A final phase of the wind-tunnel study investigated the amount of annual concentrations dispersed from the proposed stack on Building 75 given the annual release rates of 30 and 100 Ci of tritiated water vapor (HTO). Results from this simulation were compared to predictions generated by SENES Oak Ridge Inc. using the numerical dispersion code, CALPUFF. To accurately predict annual-average concentrations, both wind tunnel and numerical calculations incorporated wind data collected at the Lawrence Berkeley National Laboratory 20-meter meteorological tower located at Building 44 (see Table 1). Stack releases also were assumed to occur continuously during a day for an entire year.

CALPUFF generated predictions for an area of several kilometers extending from the site of the national laboratory. In order to produce results that are more comparable to that of CALPUFF, the wind-tunnel simulation involved concentration measurements on a grid system of 29 test points, which encompassed the entire area of the turntable model. The model area represented a full-scale diameter of 3000 ft. centered on the laboratory stack sites. Using the UC grid system, each of the 29 test points was located at each 500-ft node within a 3000 ft diameter.

Wind-tunnel simulations at each test point were conducted in correspondence to the full-scale wind speeds of 4, 10, 16, and 24 mph. According to the wind data in Table 1, a 4-mph wind was used to represent the combined wind bins with a range of 1 to 3 knots and 4 to 6 knots. The 10-mph and 16-mph winds covered the 7 to 10 knots and 11 to 16 knots, respectively, while the 24-mph wind corresponded to both the 17 to 21 knots and greater than 21 knots range. For the combined wind bins, the hours of occurrences for each wind direction were also combined. Measurements were also performed for 16 primary wind direction rotations. For each direction, concentrations were collected not only for test points that fall within a 22.5° sector downwind from the source stack but also for a few points off the sector still indicating high enough concentrations that could be significant to the annual average. Upon completion of the wind-tunnel test, all measured concentrations for each wind direction and speed settings were then converted to full-scale dilutions.

Assuming the stack releases are continuous day and night for one year and given the full-scale stack release rate of 6500 CFM, the presumed annual-average releases of 30 and 100 Ci of HTO correspond to concentrations of 3.10×10^5 and 1.03×10^6 pCi/m^3, respectively, initially emitted from the source stack. Dividing these source concentrations by the full-scale dilutions

calculated at each test point and then multiplying by the corresponding wind bin frequency for a particular direction, the fraction of HTO concentration that has reached each test location was then determined for each wind speed and direction setting. Summing these fractions from each wind speed setting resulted to an annual concentration value accumulated at each test location for a particular wind direction. The total annual concentrations generated at each test point location were then found by adding the annual concentrations contributed by each wind direction. With a grid system of calculated total annual concentrations, concentration isolines were constructed by using a linear interpolation scheme to estimate values for locations between known test locations.

Predicted concentration isolines from the wind-tunnel simulation show a slight variation to those predicted by CALPUFF. From an annual release of 30 Ci, the numerical code calculated a highest concentration of 20 pCi/m^3 would appear a few feet passed the southeast end of Building 69. The wind-tunnel method, on the other hand, predicted that the 20-pCi/m^3 ranges would occur in two areas, over the slopes of the Eucalyptus Grove and at the center of Building 69. One other significant difference shows in the trace of the 5 pCi/m^3 isoline. CALPUFF predicted that the Lawrence Hall of Science would be excluded from this concentration range, whereas, the wind-tunnel approach showed that the southern half of the complex would be exposed.

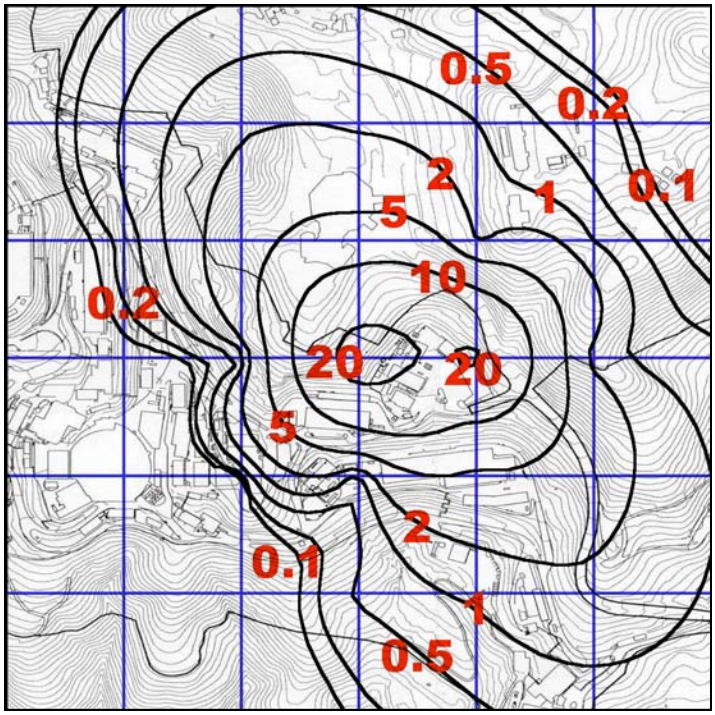

Figure 27: UC Davis Wind Tunnel predictions of annual averaged tritium concentration (pCi/m^3) isolines based on a yearly release of 30 Ci HTO.

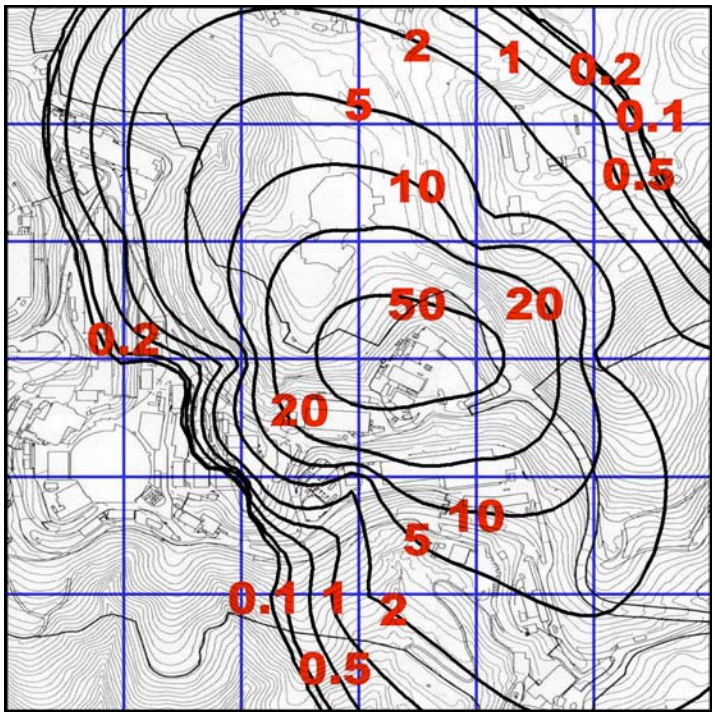

Figure 28: UC Davis Wind Tunnel predictions of annual averaged tritium concentration (pCi/m^3) isolines based on a yearly release of 100 Ci HTO.

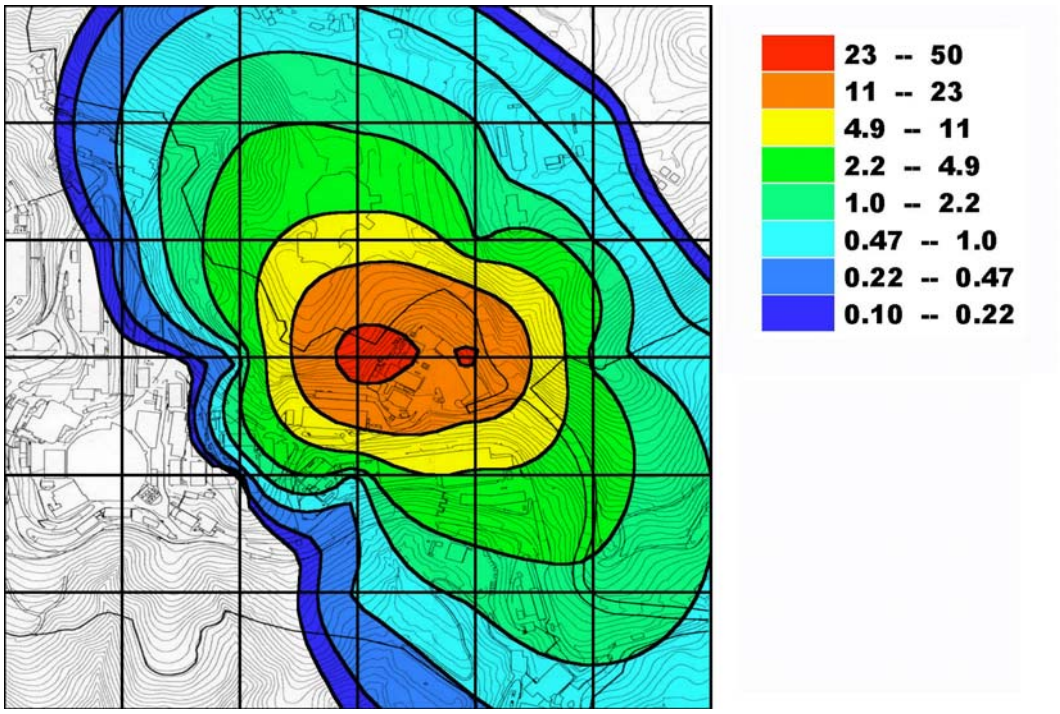

Figure 29: Multi-colored plot of UC Davis Wind Tunnel predictions of annual averaged tritium concentration (pCi/m^3) isolines based on a yearly release of 30 Ci HTO

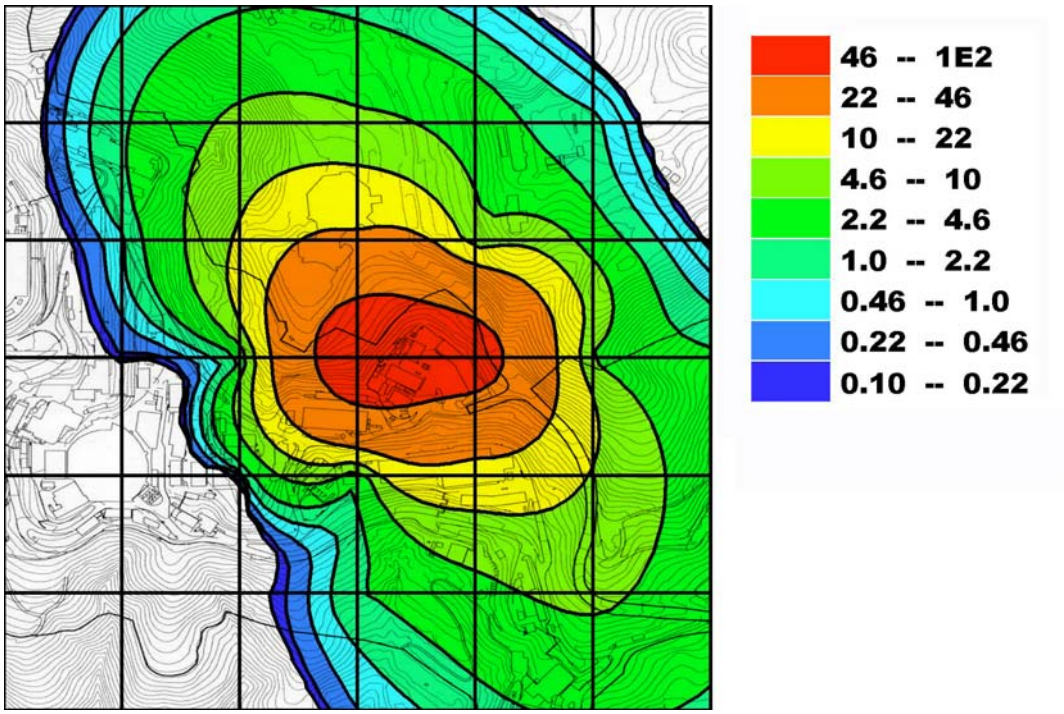

Figure 30: Multi-colored plot of UC Davis Wind Tunnel predictions of annual averaged tritium concentration (pCi/m^3) isolines based on a yearly release of 100 Ci HTO

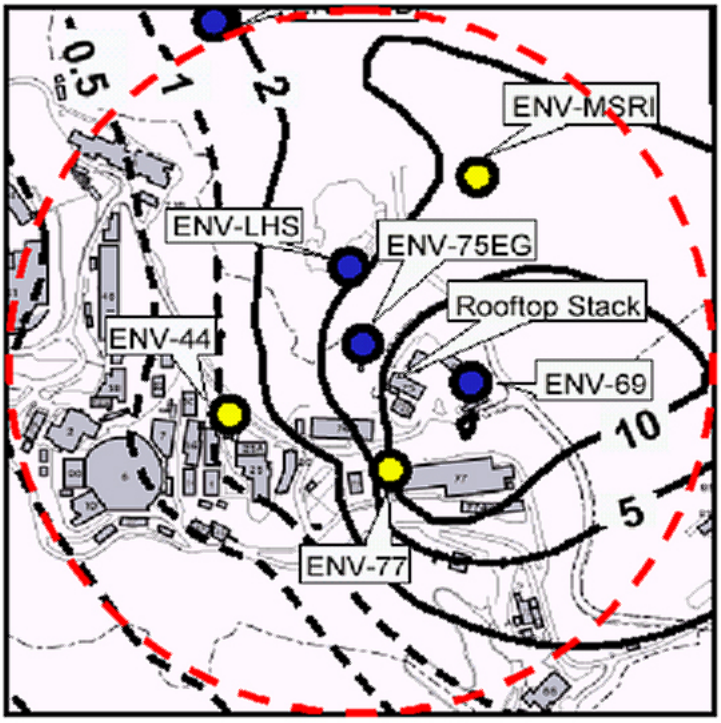

Figure 31: CALPUFF predictions of annual averaged tritium concentration (pCi/m^3) isolines based on a yearly release of 30 Ci HTO.

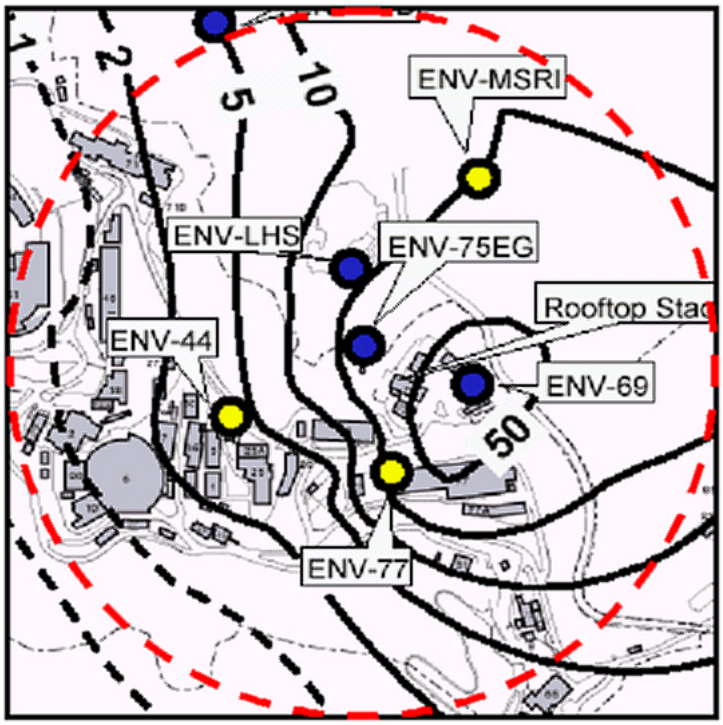

Figure 32: CALPUFF predictions of annual averaged tritium concentration (pCi/m^3) isolines based on a yearly release of 100 Ci HTO.

CONCLUSION

A wind-tunnel study was conducted for the Environmental, Health, and Safety Division of the Ernest Orlando Lawrence Berkeley National Laboratory (LBNL) to simulate stack releases of tritiated water vapor (HTO) from its National Tritium Labeling Facility (NTLF). Physical modeling simulations were performed in the Atmospheric Boundary Layer Wind Tunnel (ABLWT) at University of California, Davis. A circular-based scaled-model (1:800 inch) of the site represented a full-scale area of 3,000 feet (914 meters) in diameter, including all buildings, topography, and the relative tree cover. The model was also turntable mounted so that it could be rotated to any desired wind direction. Two stacks of different design and location were individually tested: i) an existing stack located in the same location as air sampling station ENV-75EG; and ii) a proposed stack to be built on the rooftop of Building 75. Stack effluent was modeled by releasing a neutrally buoyant tracer gas (ethane) from the scaled model exhaust system. Simultaneously, concentration (or dilution) levels of the dispersed emissions at specified downwind ground-level receptor sites were measured using a hydrocarbon gas analyzer. The wind tunnel simulated near-neutral atmospheric conditions (between stability category B and C of the Pasquill-Gifford categories). Tests were conducted over a wide range of wind regimes that dynamically matched full-scale speeds ranging from a few mph to speeds in excess of 25 mph.

Due to the complexity of the terrain, this wind-tunnel study was coordinated into three phases. An initial test was performed to determine the effects of the Berkeley site topography on the dispersion of the stack release. In order to design a complete test matrix for the site, a general understanding of the complex terrain's diversion of regions of highest concentrations must be first established. This preliminary examination was accomplished by measuring and comparing the concentration levels accumulated at a specific test point for various wind-vector rotations about the effluent source. Essentially, the technique identified the direction in which maximum concentrations were diverted due to surface topography. Over relatively flat or leveled terrains under neutral atmospheric stability, emission dispersion from a single point-source emission inherently develops a statistically Gaussian distribution of lateral concentrations with peak levels at the centerline for any distance downwind. This initial simulation showed that the downwind dispersion angle from both the existing and proposed test stacks were limited to a maximum spread of ± 22.5° from its source.

The second phase of the current study assessed the concentrations and dilution factors over a uniform grid of 49 downwind test receptors for the two most frequent wind directions blowing from the west and southeast and for three common full-scale wind speeds: 2.5, 5, and 20 mph. Both the existing stack and the proposed stack on top of Building 75 were simulated. The downwind measurement area for both stack settings was approximately 600 by 600 feet in full scale, with the test stack situated at the center of the upwind edge of the grid. Based on the measured downwind dilutions from the west wind direction setting, the existing stack's performance proved slightly better than that of the proposed stack on Building 75. For the southeasterly wind direction, the result is opposite in which the proposed stack on top of Building 75 would provide better dilution in the comparable downwind areas than the existing stack. Plots of concentration isolines would simulate routine exhaust releases for the common wind directions. The results also could be used to simulate an accidental release of non-elevated temperature effluent resulting from non-scheduled event such as a large-magnitude earthquake, human error, major equipment failure, etc. An exposure estimate could be made by knowing (or assuming) the total amount of radiation release over a specified time and then by applying the dilution factors as a function of location. For example, if 10 Ci were released continuously for one hour and a downwind area measured a full-scale concentration of 100 ppm, which corresponds to a dilution factor of 10,000, the tritium radiation concentration would be $(10 \times 10^{12}$ pCi)(100 PPM/10^6)(1 hr/11,044 m^3) = 90,547 pCi/m^3.

The third phase of wind-tunnel tests were conducted to determine the annual averaged tritium concentration in pCi/m^3 for yearly releases of 30 and 100 Ci HTO respectively. It was assumed that the release process was occurred 24 hours per day and seven days per week during an entire year. The contour isolines shown were generated from 29 individual receptors located on the intersection of the 500 feet node lines of the UC grid map in the figure. The red circular dotted line represents the physical size of the area simulated on the turntables during the testing. Figures 21 and 22 display the SENES Oak Ridge Inc. CALPUFF predictions of tritium concentration (pCi/m^3) for the same set of isoline contours based on the identical yearly releases of 30 and 100 Ci HTO, respectively. Patterns of dispersion predicted by the two approaches (CALPUFF and wind tunnel) differ slightly; however, the magnitudes of concentrations estimated by each approach are similar.

APPENDIX A:
WIND TUNNEL REDUCED DATA SETS

POINT 1 Concentrations (PPM)

UC X	UC Y
3465	875

Offset	Wind Angle	Equivalent Full-Scale Wind Speed				
(Degrees)	(Degrees)	20mph	5mph	2.5mph	0.98mph	0.5mph
-24	36	563	938	1079	1401	357
-21	39	615	954	1128	1653	671
-18	42	480	711	1072	1773	821
-15	45	397	627	928	1750	867
-12	48	544	926	1406	1682	696
-9	51	465	759	1176	1652	693
-6	54	366	647	1074	1450	773
-3	57	235	434	1074	1310	917
0	60	149	312	832	982	586
3	63	130	222	666	790	604
6	66	164	305	530	742	417
9	69	138	204	317	452	213
12	72	94	159	204	332	167

POINT 8 Concentrations (PPM)

UC X	UC Y
3475	1350

Offset	Wind Angle	Equivalent Full-Scale Wind Speed				
(Degrees)	(Degrees)	20mph	5mph	2.5mph	0.98mph	0.5mph
-12	56	115	178	214	402	188
-9	59	113	179	261	475	208
-6	62	129	190	292	596	304
-3	65	122	191	288	657	371
0	68	104	169	279	528	361
3	71	70	115	154	366	232
6	74	66	105	147	359	232
9	77	76	114	158	362	285
12	80	62	103	136	376	317

POINT 18 Concentrations (PPM)

UC X	UC Y
3400	1875

Offset	Wind Angle	Equivalent Full-Scale Wind Speed				
(Degrees)	(Degrees)	20mph	5mph	2.5mph	0.98mph	0.5mph
-12	55	68	101	159	280	209
-9	58	77	113	159	392	338
-6	61	25	79	212	445	410
-3	64	62	146	394	478	500
0	67	41	102	261	490	535
3	70	29	58	142	528	512
6	73	30	72	185	417	423
9	76	22	23	113	347	268
12	79	31	54	51	245	160

POINT 20 Concentrations (PPM)

UC X	UC Y
3527	566

Offset	Wind Angle	Equivalent Full-Scale Wind Speed				
(Degrees)	(Degrees)	20mph	5mph	2.5mph	0.98mph	0.5mph
-40	13	2959	5023	4189	1328	151
-30	23	3805	5853	7144	2072	292
-20	33	5098	8792	12063	3705	439
-10	43	6551	10087	11166	2911	325
0	53	4511	8503	10594	3081	371
10	63	5137	8707	10101	2792	328
20	73	5524	9572	9889	2359	313
30	83	4595	7367	7596	1892	197
40	93	3992	5552	5716	1246	102

Table A-1: Full-scale concentration results from Phase 1 testing.

POINT 1 dilution factors (1e6 PPM/concentration, PPM)

UC X	UC Y
3465	875

Offset	Wind Angle	Equivalent Full-Scale Wind Speed				
(Degrees)	(Degrees)	20 mph	5 mph	2.5 mph	0.98 mph	0.5 mph
-24	36	1775	1066	927	714	2797
-21	39	1627	1049	887	605	1490
-18	42	2084	1406	933	564	1218
-15	45	2519	1594	1078	571	1154
-12	48	1838	1079	711	595	1438
-9	51	2151	1317	850	605	1442
-6	54	2735	1547	931	690	1294
-3	57	4251	2304	931	763	1090
0	60	6710	3203	1202	1019	1705
3	63	7666	4509	1502	1266	1655
6	66	6102	3274	1888	1348	2398
9	69	7234	4902	3159	2212	4697
12	72	10679	6273	4902	3012	5980

POINT 8 dilution factors (1e6 PPM/concentration, PPM)

UC X	UC Y
3475	1350

Offset	Wind Angle	Equivalent Full-Scale Wind Speed				
(Degrees)	(Degrees)	20mph	5mph	2.5mph	0.98mph	0.5mph
-12	56	8709	5606	4672	2485	5308
-9	59	8882	5572	3833	2106	4797
-6	62	7733	5277	3424	1677	3286
-3	65	8230	5246	3477	1523	2694
0	68	9646	5902	3588	1892	2769
3	71	14239	8709	6500	2735	4313
6	74	15204	9543	6796	2786	4313
9	77	13192	8794	6317	2760	3504
12	80	16018	9750	7353	2662	3159

POINT 18 dilution factors (1e6 PPM/concentration, PPM)

UC X	UC Y
3400	1875

Offset	Wind Angle	Equivalent Full-Scale Wind Speed				
(Degrees)	(Degrees)	20mph	5mph	2.5mph	0.98mph	0.5mph
-12	55	14785	9896	6304	3570	4785
-9	58	13067	8826	6284	2553	2955
-6	61	39709	12706	4725	2248	2436
-3	64	16198	6836	2540	2092	1999
0	67	24257	9771	3835	2041	1868
3	70	33953	17129	7020	1892	1954
6	73	33609	13798	5397	2398	2367
9	76	45814	43398	8855	2884	3738
12	79	32279	18496	19616	4078	6266

POINT 20 dilution factors (1e6 PPM/concentration, PPM)

UC X	UC Y
3527	566

Offset	Wind Angle	Equivalent Full-Scale Wind Speed				
(Degrees)	(Degrees)	20mph	5mph	2.5mph	0.98mph	0.5mph
-40	13	338	199	239	753	6630
-30	23	263	171	140	483	3426
-20	33	196	114	83	270	2279
-10	43	153	99	90	343	3080
0	53	222	118	94	325	2698
10	63	195	115	99	358	3047
20	73	181	104	101	424	3197
30	83	218	136	132	529	5082
40	93	250	180	175	803	9826

Table A-2: Dilution factor results from Phase 1 testing.

WEST WIND DIRECTION					SOUTHEAST WIND DIRECTION				
Grid Coordinates		Full-scale concentrations acquired at the following wind speeds			Grid Coordinates		Full-scale concentrations acquired at the following wind speeds		
UC East [feet]	UC North [feet]	2.5 mph	5 mph	20 mph	UC East [feet]	UC North [feet]	2.5 mph	5 mph	20 mph
3550	220	0	5.0047	28.4848	2913.61	732.13	37.2193	15.2889	0.7735
3550	320	12.6605	4.7042	27.9111	2984.32	802.84	229.6394	231.449	85.5854
3550	420	14.9416	8.7668	49.4871	3055.03	873.55	605.9907	395.5228	191.7511
3550	520	957.9433	3139.9089	11627.4229	3125.74	944.26	806.8955	558.3431	252.4879
3550	620	43.2199	47.5762	73.2488	3196.45	1014.97	220.7313	189.9099	35.8507
3550	720	5.7481	14.9979	41.2973	3267.16	1085.68	34.1965	22.8597	0
3550	820	8.3236	2.258	30.3606	3337.87	1156.39	0	0	0
3650	220	1.522	6.4016	31.2466	2984.32	661.42	0	3.3078	37.396
3650	320	3.4961	1.7756	34.5485	3055.03	732.13	344.2897	384.0248	237.5694
3650	420	22.9489	37.5633	88.2252	3125.74	802.84	1326.693	962.585	573.3105
3650	520	101.0927	53.8665	99.6661	3196.45	873.55	1011.708	641.4114	361.545
3650	620	63.3596	22.7711	51.778	3267.16	944.26	86.3417	108.189	43.2907
3650	720	26.4527	8.1312	34.8221	3337.87	1014.97	0	4.387	0
3650	820	9.7276	3.9735	29.0737	3408.58	1085.68	0	0	0
3750	220	1.4022	0	28.6856	3055.03	590.71	0	0	0
3750	320	12.0857	0	37.3036	3125.74	661.42	48.7787	149.6137	79.3769
3750	420	74.4857	50.1891	98.0904	3196.45	732.13	1865.973	1310.038	772.6074
3750	520	126.2763	60.5749	112.8093	3267.16	802.84	1171.857	677.1502	461.6347
3750	620	63.0132	26.4175	54.0738	3337.87	873.55	37.7312	67.474	20.6771
3750	720	8.6807	11.864	35.2466	3408.58	944.26	0	0	0
3750	820	4.1599	0	32.0628	3479.29	1014.97	0	0	0
3850	220	0	0	41.2692	3125.74	520	0	1.2054	0
3850	320	11.006	0	62.5841	3196.45	590.71	36.1914	83.8561	0
3850	420	160.5558	36.6751	126.0791	3267.16	661.42	1700.309	1497.9257	820.1877
3850	520	214.1577	52.8444	90.2101	3337.87	732.13	1894.403	1055.0243	612.1759
3850	620	103.1722	6.9475	57.6547	3408.58	802.84	0.2345	53.1808	0
3850	720	18.25	7.629	32.3844	3479.29	873.55	0	1.0863	0
3850	820	0	1.2725	33.0988	3550	944.26	0	0	0
3950	220	19.6167	0	48.1493	3196.45	449.29	0	1.1228	0.7991
3950	320	166.6316	31.3949	113.0076	3267.16	520	0	51.6504	22.4895
3950	420	376.186	137.6645	142.1378	3337.87	590.71	1235.606	873.6055	484.1277
3950	520	369.8287	107.8632	105.6453	3408.58	661.42	3227.354	2183.6838	1489.9448
3950	620	127.9562	1.9062	49.3095	3479.29	732.13	24.6798	65.7675	73.5952
3950	720	15.4222	0	32.5131	3550	802.84	0	8.4065	12.9958
3950	820	2.252	0	30.7238	3620.71	873.55	0	2.5228	1.1974
4050	220	37.1047	0	67.278	3267.16	378.58	0	5.9067	2.4124
4050	320	110.3281	40.6199	103.2681	3337.87	449.29	0	17.078	91.664
4050	420	314.7347	137.8244	123.8872	3408.58	520	941.3272	1023.3129	845.2417
4050	520	408.4853	130.6634	89.5959	3479.29	590.71	4400.79	3289.7942	2594.5271
4050	620	142.0413	0	46.7364	3550	661.42	16.0422	83.5435	41.3484
4050	720	26.3675	0	32.4294	3620.71	732.13	0	3.5421	0.5983
4050	820	1.5812	0	30.1662	3691.42	802.84	0	2.4935	0
4150	220	91.9829	23.0827	45.2056	3337.87	307.87	0	7.301	3.6377
4150	320	231.0544	45.8734	101.5267	3408.58	378.58	0	7.4983	3.448
4150	420	445.511	141.4612	133.5632	3479.29	449.29	0	29.882	35.1168
4150	520	451.2755	174.5189	115.1188	3550	520	896.2112	5002.8721	7244.7905
4150	620	292.7032	80.1045	80.9193	3620.71	590.71	0	5.5811	19.3428
4150	720	0	0	10.6629	3691.42	661.42	0	0.6374	0
4150	820	0	0	12.1122	3762.13	732.13	0	0	0.3819

Table A-3: Full-scale concentrations for Phase 2 existing stack concentration isoline plots.

WEST WIND DIRECTION

Grid Coordinates UC East [feet]	Grid Coordinates UC North [feet]	Full-scale concentrations acquired at the following wind speeds 2.5 mph	5 mph	20 mph
3650	120	0	0	11.8433
3650	220	0	0	12.4973
3650	320	0	0	10.9255
3650	420	233.829	404.5946	1480.3859
3650	520	193.5711	261.8797	277.7997
3650	620	157.647	160.2586	250.4707
3650	720	32.3862	53.0292	163.9904
3750	120	0	0	137.0587
3750	220	2.7349	0	139.0234
3750	320	22.3166	23.4487	147.722
3750	420	270.7855	340.3889	159.1502
3750	520	318.1409	397.041	423.885
3750	620	51.0073	132.9839	140.5733
3750	720	0	4.3025	56.5933
3850	120	0	0	136.709
3850	220	31.644	6.6274	136.9219
3850	320	126.0943	74.5541	134.1334
3850	420	428.3644	484.4723	128.503
3850	520	379.9817	514.9795	90.7486
3850	620	53.5876	80.1699	82.8089
3850	720	0	40.0559	110.5086
3950	120	0	0	26.1513
3950	220	58.3694	20.8568	29.4475
3950	320	532.7753	307.7647	34.1484
3950	420	770.2997	607.2737	43.0271
3950	520	381.8429	331.1201	64.2366
3950	620	24.111	39.1568	81.917
3950	720	0	0	106.7907
4050	120	5.0452	0	0
4050	220	166.675	73.5128	0
4050	320	434.4309	213.9315	19.8392
4050	420	594.5255	393.8885	68.663
4050	520	386.9624	270.6893	124.7821
4050	620	25.919	29.9369	18.1954
4050	720	0.2848	0	0
4150	120	53.4492	22.63	0
4150	220	291.0136	134.0048	0
4150	320	498.2838	231.1396	27.5114
4150	420	594.6782	325.3308	59.9723
4150	520	459.9652	297.2203	92.5381
4150	620	251.2198	165.3617	76.1622
4150	720	6.4998	2.1924	0
4250	120	138.4637	61.7707	0
4250	220	345.1719	196.0614	2.8264
4250	320	528.9118	277.4188	28.3257
4250	420	600.2564	355.2933	69.2653
4250	520	427.3269	289.9686	95.3291
4250	620	280.4075	176.005	79.1282
4250	720	59.9469	54.4416	8.3469

SOUTHEAST WIND DIRECTION

Grid Coordinates UC East [feet]	Grid Coordinates UC North [feet]	Full-scale concentrations acquired at the following wind speeds 2.5 mph	5 mph	20 mph
2913.61	732.13	45.2598	0	0
2984.32	802.84	229.9544	52.0465	0
3055.03	873.55	526.2523	166.1145	9.791
3125.74	944.26	855.7981	323.1226	47.8029
3196.45	1014.97	442.7343	164.5955	15.0309
3267.16	1085.68	123.3696	17.3509	0
3337.87	1156.39	41.2755	0	0
2984.32	661.42	37.6804	39.0992	20.7901
3055.03	732.13	295.1379	167.2651	37.3433
3125.74	802.84	997.8823	447.9844	90.6998
3196.45	873.55	1023.702	442.195	110.8317
3267.16	944.26	546.0083	194.3252	63.3234
3337.87	1014.97	144.5033	31.5429	0.0436
3408.58	1085.68	59.5252	0	0
3055.03	590.71	54.0351	33.1253	17.1703
3125.74	661.42	372.5739	163.2884	65.5918
3196.45	732.13	1116.999	526.3361	102.4749
3267.16	802.84	999.7121	537.0517	74.7461
3337.87	873.55	377.9774	301.8033	33.2983
3408.58	944.26	90.2168	68.4112	0
3479.29	1014.97	33.5912	36.6454	0
3125.74	520	25.7607	41.5576	0
3196.45	590.71	165.9779	181.9268	10.1499
3267.16	661.42	1131.476	663.002	100.7841
3337.87	732.13	1328.526	691.4989	105.1821
3408.58	802.84	514.3052	278.5736	30.587
3479.29	873.55	66.3842	86.3498	0
3550	944.26	39.3702	60.948	0
3196.45	449.29	28.3768	26.6947	0
3267.16	520	178.2223	130.4553	18.8471
3337.87	590.71	1062.969	678.3801	146.2182
3408.58	661.42	1538.525	998.5977	188.3147
3479.29	732.13	441.5102	338.7609	74.0794
3550	802.84	148.138	207.255	14.9869
3620.71	873.55	38.2807	66.6716	0
3267.16	378.58	37.6456	48.172	0
3337.87	449.29	73.3947	112.0379	7.2983
3408.58	520	1012.954	824.1015	128.4701
3479.29	590.71	1810.647	1096.3644	184.5451
3550	661.42	500.3123	506.8128	111.7072
3620.71	732.13	151.9264	162.9768	20.4395
3691.42	802.84	67.5558	93.4591	0
3337.87	307.87	24.802	45.9938	0
3408.58	378.58	77.9561	121.0456	69.0881
3479.29	449.29	405.3115	413.2711	174.1949
3550	520	1600.643	1814.217	464.2316
3620.71	590.71	498.181	793.8242	199.7098
3691.42	661.42	165.5082	239.7591	89.4177
3762.13	732.13	91.3522	113.6594	21.5127
3408.58	237.16	0	0	0
3479.29	307.87	46.5783	101.3751	0
3550	378.58	166.1892	447.1773	342.1955
3620.71	449.29	417.1565	1010.8409	1385.2262
3691.42	520	140.5497	294.5905	358.2977
3762.13	590.71	90.2551	163.0463	158.7897
3832.84	661.42	64.8051	97.5411	

Table A-4: Full-scale concentrations for Phase 2 proposed Bldg 75 stack concentration isolines.

Grid Coordinates and Overall Concentration Inputs for Contour Plot

Conversion from UC Grid to UTM Coordinates
UC Grid Ref Points (Hearst Mining Circle = 0,0)
UTME = 565448
UTMN = 4191869
Correction Angle = 16.71666667 degrees

Presumed toxic emission per year = 30 Ci/yr

	Receptor Location				Overall Total
Receptor	UC Coordinates		UTM Coordinates		Concentrations
Number	East (ft)	North (ft)	UTME	UTMN	[pCi/m^3]
1	3500	2000	566294	4192760	0.4918
2	4500	1500	566630	4192701	0.4003
3	4000	1500	566484	4192658	1.0334
4	3500	1500	566338	4192614	1.7317
5	3000	1500	566192	4192570	1.8194
6	2500	1500	566046	4192526	0.5339
7	4500	1000	566674	4192555	0.9353
8	4000	1000	566528	4192512	1.4303
9	3500	1000	566382	4192468	6.5466
10	3000	1000	566236	4192424	3.2835
11	2500	1000	566090	4192380	0.2380
12	5000	500	566864	4192453	0.7032
13	4500	500	566718	4192409	1.1030
14	4000	500	566572	4192366	22.3736
15	3500	500	566426	4192322	27.3706
16	3000	500	566280	4192278	0.1082
17	2500	500	566134	4192234	0.0741
18	2000	500	565988	4192190	0.0575
19	4500	0	566762	4192264	2.8765
20	4000	0	566616	4192220	4.3226
21	3500	0	566470	4192176	0.3181
22	3000	0	566324	4192132	0.0801
23	2500	0	566178	4192088	0.0508
24	4500	-500	566805	4192118	1.8188
25	4000	-500	566660	4192074	1.1184
26	3500	-500	566514	4192030	0.6083
27	3000	-500	566368	4191986	0.0462
28	2500	-500	566222	4191942	0.0132
29	3500	-1000	566557	4191884	0.1533
30	3937.5	250	566576	4192287	10.5282

Table A-5: Annual average concentrations based on a 30 Ci annual release for Phase 3 concentration isoline plots.

Grid Coordinates and Overall Concentration Inputs for Contour Plot

Conversion from UC Grid to UTM Coordinates
UC Grid Ref Points (Hearst Mining Circle = 0,0)
UTME = 565448
UTMN = 4191869
Correction Angle = 16.71666667 degrees

Presumed toxic emission per year = 100 Ci/yr

	Receptor Location				Overall Total
Receptor	UC Coordinates		UTM Coordinates		Concentrations
Number	East (ft)	North (ft)	UTME	UTMN	[pCi/m^3]
1	3500	2000	566294	4192760	1.6392
2	4500	1500	566630	4192701	1.3342
3	4000	1500	566484	4192658	3.4446
4	3500	1500	566338	4192614	5.7724
5	3000	1500	566192	4192570	6.0648
6	2500	1500	566046	4192526	1.7796
7	4500	1000	566674	4192555	3.1178
8	4000	1000	566528	4192512	4.7678
9	3500	1000	566382	4192468	21.8219
10	3000	1000	566236	4192424	10.9451
11	2500	1000	566090	4192380	0.7933
12	5000	500	566864	4192453	2.3439
13	4500	500	566718	4192409	3.6766
14	4000	500	566572	4192366	74.5785
15	3500	500	566426	4192322	91.2352
16	3000	500	566280	4192278	0.3605
17	2500	500	566134	4192234	0.2470
18	2000	500	565988	4192190	0.1918
19	4500	0	566762	4192264	9.5883
20	4000	0	566616	4192220	14.4086
21	3500	0	566470	4192176	1.0604
22	3000	0	566324	4192132	0.2669
23	2500	0	566178	4192088	0.1695
24	4500	-500	566805	4192118	6.0625
25	4000	-500	566660	4192074	3.7279
26	3500	-500	566514	4192030	2.0276
27	3000	-500	566368	4191986	0.1539
28	2500	-500	566222	4191942	0.0440
29	3500	-1000	566557	4191884	0.5110
30	3937.5	250	566576	4192287	35.0940

Table A-6: Annual average concentrations based on a 100 Ci annual release for Phase 3 concentration isoline plots.

APPENDIX B:
THE ATMOSPHERIC BOUNDARY LAYER WIND TUNNEL AT UNIVERSITY OF CALIFORNIA, DAVIS

In the present investigation, the Atmospheric Boundary Layer Wind Tunnel (ABLWT) located at University of California, Davis was used (Figure B-1). Built in 1979 the wind tunnel was originally designed to simulate turbulent boundary layers comparable to wind flow near the surface of the earth. In order to achieve this effect, the tunnel requires a long flow-development section such that a mature boundary-layer flow is produced at the test section. The wind tunnel is an open-return type with an overall length of 21.3 m and is composed of five sections: the entrance, the flow-development section, the test section, the diffuser section, and the fan and motor.

The entrance section is elliptical in shape with a smooth contraction area that minimizes the free-stream turbulence of the incoming flow. Following the contraction area is a commercially available air filter that reduces large-scale pressure fluctuations of the flow and filters larger-size particles out of the incoming flow. Behind the filter, a honeycomb flow straightener is used to reduce large-scale turbulence.

The flow development section is 12.2 m long with an adjustable ceiling for longitudinal pressure-gradient control. For the present study, the ceiling was diverged ceiling so that a zero-pressure-gradient condition is formed in the stream wise direction. At the leading edge of the section immediately following the honeycomb flow straightener, four triangularly shaped spires are stationed on the wind-tunnel floor to provide favorable turbulent characteristics in the boundary-layer flow. Roughness elements are then placed all over the floor of this section to artificially thicken the boundary layer. For a free-stream wind speed of 4.0 m/s, the wind-tunnel boundary layer grows to a height of one meter at the test section. With a thick boundary layer, larger models could be tested and thus measurements could be made at higher resolution.

Dimensions of the test section are 2.44 m in stream wise length, 1.66 m high, and 1.18 m wide. Similar to the flow-development section, the test section ceiling can also be adjusted to obtain the desired stream wise pressure gradient. Experiments can be observed from both sides of the test section through framed Plexiglas windows. One of the windows is also a sliding door that allows access into the test section. When closed twelve clamps distributed over the top and lower edges are used to seal the door. Inside the test section, a three-dimensional probe-

positioning system is installed at the ceiling to provide fast and accurate sensor placement. The traversing system scissor-type extensions, which provide vertical probe motion, are also made of aerodynamically shaped struts to minimize flow disturbances.

The diffuser section is 2.37 m long and has an expansion area that provides a continuous transition from the rectangular cross-section of the test section to the circular cross-sectional area of the fan. To eliminate upstream swirl effects from the fan and avoid flow separation in the diffuser section, fiberboard and honeycomb flow straighteners are placed between the fan and diffuser sections.

The fan consists of eight constant-pitch blades 1.83 m in diameter and is powered by a 56 kW (75 hp) variable-speed DC motor. A dual belt and pulley drive system is used to couple the motor and the fan.

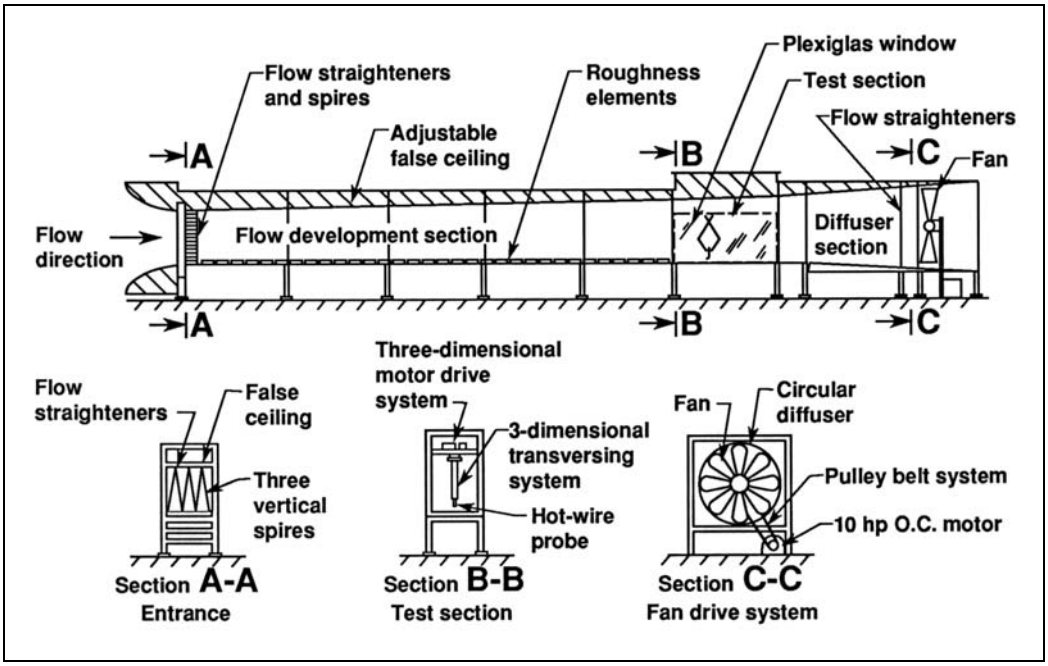

Figure B-1: Schematic diagram of the UC Davis Atmospheric Boundary Layer Wind Tunnel.

APPENDIX C:
INSTRUMENTATION AND MEASUREMENT SYSTEMS

Wind tunnel measurements of the mean velocity and turbulence characteristics were performed using hot-wire anemometry. A standard Thermo Systems Inc. (TSI) single hot-wire sensor model 1210-60 was used to measure the wind quantities. The sensor was installed at the end of a TSI model 1150 50-cm probe support, which was secured onto the support plate of the three-dimensional sensor positioning system in the U.C. Davis Atmospheric Boundary Layer Wind Tunnel (ABLWT) test section. A 10-m shielded tri-axial cable was then used to connect the probe support and sensor arrangement to a TSI model IFA 100 constant temperature thermal-anemometry unit with signal conditioner.

Hot-wire sensor calibrations were conducted in the ABLWT test section over the range of common velocities measured in the wind-tunnel boundary layer. Signal-conditioned voltage readings of the hot-wire sensor were then matched against the velocity measurements from a Pitot-static tube connected to a Meriam model 34FB2 oil micro-manometer, which had a resolution of 25.4 μm of oil level. The specific gravity of the oil was 0.934. The Pitot-static tube was secured to an aerodynamically shaped stand and was positioned so that its flow-sensing tip is normal to the flow and situated near the volumetric center of the test section. Normal to the flow, the end of the hot-wire sensor was then traversed to a position 10 cm next to the tip of the Pitot-static tube.

Concentration measurements of an ethane tracer gas were conducted with the use of a Rosemount Analytical model 400A hydrocarbon analyzer. This instrument uses a flame-ionization detection method to determine trace concentrations in the air. Operation of this analyzer involves iso-kinetically aspirating ethane-air samples into a burner where the sample is burned with a mixture of medical-rated air and 40% hydrogen and 60% nitrogen. Figure C-1 displays a schematic of the concentration measurement system. A 1/4-inch-diameter, copper refrigeration-grade tubing, 12 inches in length, was used as the gas-analyzer sensing probe, mitered 45° at the end. This copper probe was secured to the test-section traverse-system mounting plate, where an additional length of the same type tubing was used to connect the probe to a pressure-regulated vacuum pump, which sends samples into the analyzer at a constant pressure of 5 psig.

Calibration of the hydrocarbon analyzer system was accomplished with two known samples of ethane-air mixtures, one certified with 52.4 parts per million (ppm) and the other with 524.8 ppm. Calibration gas samples were accurate to less than 0.5% of the stated value. The precision of the gas analyzer was within 1% of full scale. Prior to the calibration, the analyzer voltage output was first mechanically zeroed using a sample of pure air (hydrocarbon-free).

Ethane tracer gas emissions from the stacks were controlled by a model B-250-1 ball-type flow meter. Flow meter volumetric flow rates for a tracer gas of some ethane mixture are calibrated by measuring the time elapsed for the tracer gas to fill a container of known volume. Since the ethane mixture was virtually invisible, the gas level needs to be monitored by using a traceable substance such as water. This was done by first filling and completely submerging the calibration container in a water tank. The ethane gas mixture is released in the container by inserting a tube extension from the flow meter into the water-drowned container. A complete fill of tracer gas can then be detected when the decreasing water level reaches the mark corresponding to a known volume. For a thorough calibration, elapsed times are collected for at least three height settings on the flow meter gage. Dividing these times by the known volume gives a volumetric flow rate for a corresponding flow meter height setting.

Raw voltage data sets of hot-wire velocity measurements and of tracer gas concentrations were digitally collected using a LabVIEW data acquisition system, which was installed in a Gateway personal computer with a Pentium 166Mhz processor. Concentration voltages were collected from the hydrocarbon analyzer analog output, while hot wire voltages were obtained from the signal conditioner output of the IFA 100 anemometer. The two outputs were connected to a multi-channel daughter board linked to a United Electronics Inc. (UEI) analog-to-digital (A/D) data acquisition board, which is installed in one of the ISA motherboard slots of the Gateway PC. LabVIEW software was used to develop virtual instruments (VI) that would initiate and configure the A/D board, then collect the voltage data given by the measurement equipment, display appropriately converted results on the computer screen, and finally save the raw voltage data into a designated filename.

Since velocity and concentration measurements were individually performed, a VI was developed for each type of acquisition. For the hot-wire acquisition, the converted velocity data and its histogram is displayed along with the mean voltages, mean velocity, root-mean-square velocity, and turbulence intensity. In the concentration VI, the converted concentration data is

shown with the corresponding mean voltage and mean concentration. For both programs, the raw voltage data can be saved in the computer hard drive. For both hot-wire and concentration acquisition 30,000 samples were collected at a sampling rate of 1000 Hz. This acquisition setting greatly satisfies the Nyquist sampling theorem such that the average tunnel turbulence signal was 300 Hz.

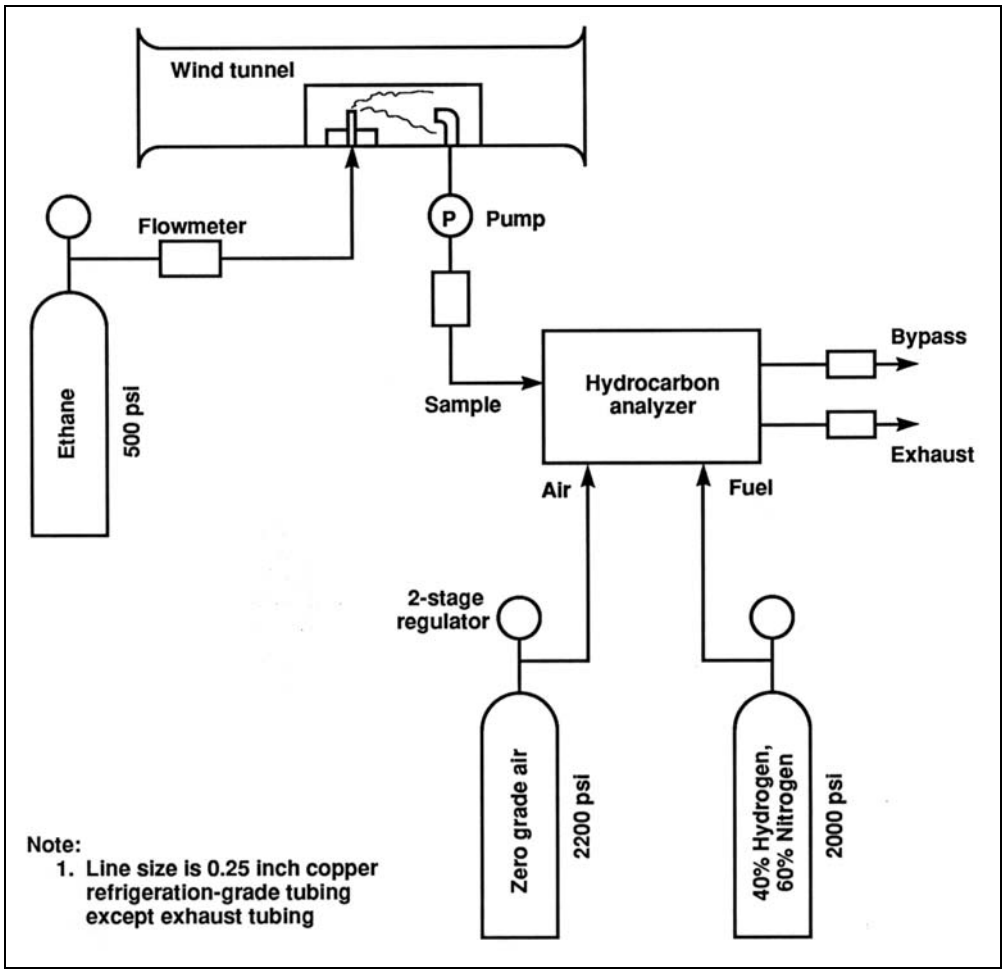

Figure C-1: Schematic diagram of gas dispersion concentration measurement system.

APPENDIX D:
WIND-TUNNEL ATMOSPHERIC FLOW SIMILARITY PARAMETERS

Wind-tunnel models of a particular test site are typically several orders of magnitude smaller than the full-scale size. In order to appropriately simulate atmospheric winds in the U.C. Davis Atmospheric Boundary Layer Wind Tunnel (ABLWT), certain flow parameters must be satisfied between a model and its corresponding full-scale equivalent. Similitude parameters can be obtained by non-dimensionalizing the equations of motion, which build the starting point for the similarity analysis. Fluid motion can be described by the following time-averaged equations.

Conservation of mass:

$$\frac{\partial \overline{U}_i}{\partial t_i} = 0 \text{ and } \frac{\partial \rho}{\partial t} + \frac{\partial (\rho \overline{U}_i)}{\partial x_i} = 0$$

Conservation of momentum:

$$\frac{\partial \overline{U}_i}{\partial t} + \overline{u}\ \frac{\partial \overline{U}_i}{\partial x_j} + 2\varepsilon_{ijk}\Omega_j \overline{U}_k = -\frac{1}{\rho_0}\frac{\partial \overline{\delta P}}{\partial x_i} - \frac{\overline{\delta T}}{T_0} g\delta_{i3} + \nu_0 \frac{\partial^2 \overline{U}_i}{\partial x_j} + \frac{\partial (\overline{-u_j u_i})}{\partial x_j}$$

Conservation of energy:

$$\frac{\partial \overline{\delta T}}{\partial t} + \overline{U}_i \frac{\partial \overline{\delta T}}{\partial x_i} = \left[\frac{\kappa_0}{\rho_0 c_{p_0}}\right] \frac{\partial^2 \overline{\delta T}}{\partial x_k \partial x_k} + \frac{\partial (-\overline{\theta u_i})}{\partial x_i} + \frac{\overline{\phi}}{\rho_0 c_{p_0}}$$

Here, the mean quantities are represented by capital letters while the fluctuating values by small letters. δP is the deviation of pressure in a neutral atmosphere. ρ_0 and T_0 are the density and temperature of a neutral atmosphere and ν_0 is the kinematic viscosity. In the equation for the conservation of energy, ϕ is the dissipation function, $\overline{\delta T}$ is the deviation of temperature from the temperature of a neutral atmosphere, κ_0 is the thermal diffusivity, and c_{p_o} is the heat capacity.

Applying the Boussinesq density approximation, application of the equations is then restricted to fluid flows where $\overline{\delta T} << T_0$. Defining the following non-dimensional quantities and then substituting into the above equations.

$$\overline{U}_i' = \overline{U}_i' \Big/ U_0 \ ;\ u_i' = u_i \Big/ U_0 \ ;\ x_i' = x_i \Big/ L_0 \ ;\ t' = tU_0 \Big/ L_0 \ ;\ \Omega_j' = \Omega_j \Big/ \Omega_0 \ ;\ \overline{\delta P}' = \overline{\delta P} \Big/ \rho_0 U_0^2 \ ;$$

$$\overline{\delta T}' = \overline{\delta T} \Big/ \delta T_0 \ ;\ g' = g \Big/ g_0 \ ;\ \overline{\varphi}' = \overline{\varphi} \Big/ \varphi_0$$

The equations of motion can be presented in the following dimensionless forms.

Continuity Equation:

$$\frac{\partial u_i'}{\partial k_i'} = 0 \text{ and } \frac{\partial \rho'}{\partial t'} + \frac{\partial (\rho' u_i')}{\partial x_i'} = 0$$

Momentum Equation:

$$\frac{\partial \overline{U}_i'}{\partial t'} + \overline{U}_j' \frac{\partial \overline{U}_i'}{\partial x_j'} + \frac{2}{Ro} \varepsilon_{ijk} \overline{U}_k' \Omega_j' = -\frac{\partial \overline{\delta P}'}{\partial x_i'} + \frac{1}{Fr^2} \overline{\delta T}' \delta_{3i} + \frac{1}{Re} \frac{\partial^2 \overline{U}_i'}{\partial x_j' \partial x_j'} + \frac{\partial (\overline{-u_j' u_i'})}{\partial x_j'}$$

Turbulent Energy Equation:

$$\frac{\partial \overline{\delta T}'}{\partial t'} + \overline{U}_i' \frac{\partial \overline{\delta T}'}{\partial x_i'} = Pr \cdot \frac{1}{Re} \frac{\partial^2 \overline{\delta T}'}{\partial x_k' \partial x_k'} + \frac{\partial (-\overline{\theta' u_i'})}{\partial x_i'} + \frac{1}{Re} \cdot Ec \cdot \overline{\varphi}'$$

Although the continuity equation gives no similarity parameters, coefficients from both other equations do provide the following desired similarity parameters.

1. Rossby number: $R_0 \equiv U_0 / L_0 \Omega_0$

2. Densimetric Froude number: $Fr \equiv U_0 / (g L_0 \delta T_0 / T_0)^{1/2}$

3. Prandtl number: $Pr \equiv \rho_0 c_{p_0} \nu_0 / \kappa_0$

4. Eckert number: $Ec \equiv U_0^2 / c_{p_0} \delta T_0$

5. Reynolds number: $Re \equiv U_0 L_0 / \nu_0$

In the dimensionless momentum equation, the Rossby number is extracted from the denominator of the third term on the left hand side. The Rossby number represents the ratio of advective acceleration to Coriolis acceleration due to the rotation of the earth. If the Rossby number is large, Coriolis accelerations are small. Since UC Davis ABLWT is not rotating, the Rossby number is infinite allowing the corresponding term in the dimensionless momentum equation to approach zero. In nature, however, the rotation of the earth influences the upper layers of the atmosphere; thus, the Rossby number is small and becomes important to match, and the corresponding term in the momentum equation is sustained.

Most modelers have assumed the Rossby number to be large, thus, neglecting the respective term in the equations of motion and ignoring the Rossby number as a criterion for modeling. Snyder (1981) showed that the characteristic length scale, L_0, must be smaller than 5 km in order to simulate diffusion under neutral or stable conditions in relatively flat terrain. Other researchers discovered similar findings. Since UC Davis ABLWT produces a boundary layer with a height of about one meter, the surface layer vertically extends 10 to 15 cm above the ground. In this region the velocity spectrum would be accurately modeled. The Rossby number can then be ignored in this region. Since testing is limited to the lower 10% to 15% of the boundary layer, the length in longitudinal direction, which can be modeled, has to be no more than a few kilometers.

Derived from the denominator of the second term on the right hand side of the dimensionless momentum equation, the square of the Froude number represents the ratio of inertial forces to buoyancy forces. High values of the Froude number infer that the inertial forces are dominant. For values equal or less than unity, thermal effects become important. Since the conditions inside the UC Davis ABLWT are inherently isothermal, the wind tunnel generates a neutrally stable boundary layer; hence, the Froude number is infinitely large allowing the respective term in the momentum equation to approach zero.

The third parameter is the Prandtl number, which is automatically matched between the wind-tunnel flow and full-scale winds if the same fluid is been used. The Eckert number criterion is important only in compressible flow, which is not of interest for a low-speed wind tunnel.

Reynolds number represents the ratio of inertial to viscous forces. The reduced scale of a wind tunnel model results in a Reynolds number several orders of magnitude smaller than in full scale. Thus, viscous forces are more dominant in the model than in nature. No atmospheric flow could be modeled, if strict adherence to the Reynolds number criterion was required. However, several arguments have been made to justify the use of a smaller Reynolds number in a model. These arguments include laminar flow analogy, Reynolds number independence, and dissipation scaling. With the absence of thermal and Coriolis effects, several test results have shown that the scaled model flow will be dynamically similar to the full-scale case if a critical Reynolds number is larger than a minimum independence value. The gross structure of turbulence is similar over a wide range of Reynolds numbers. Nearly all modelers use this approach today.

APPENDIX E:
WIND-TUNNEL ATMOSPHERIC BOUNDARY-LAYER SIMILARITY

Wind-tunnel simulation of the atmospheric boundary layer under neutrally stable conditions must also meet non-dimensional boundary-layer similarity parameters between the scaled-model flow and its full-scale counterpart. The most important conditions are:

1. The normalized mean velocity, turbulence intensity, and turbulent energy profiles.
2. The roughness Reynolds number, $\mathrm{Re}_z = z_0 u_* / \nu$.
3. Jensen's length-scale criterion of z_0/H.
4. The ratio of H/δ for H greater than $H/\delta > 0.2$.

In the turbulent core of a neutrally stable atmospheric boundary layer, the relationship between the local flow velocity, U, versus its corresponding height, z, may be represented by the following velocity-profile equation.

$$\frac{U}{U_\infty} = \left(\frac{z}{\delta}\right)^\alpha$$

Here, U_∞ is the mean velocity of the inviscid flow above the boundary layer, δ is the height of the boundary layer, and α is the power-law exponent, which represents the upwind surface conditions. Wind-tunnel flow can be shaped such that the exponent α will closely match its corresponding full-scale value, which can be determined from field measurements of the local winds. The required power-law exponent, α, can then be obtained by choosing the appropriate type and distribution of roughness elements over the wind tunnel flow-development section.

Full-scale wind data suggest that the atmospheric wind profile at the site of the Lawrence Berkeley National Laboratory yields a nominal value of $\alpha = 0.3$. This condition was closely matched in the UC Davis Atmospheric Boundary Layer Wind Tunnel by systematically arranging an pattern of 2" x 4" wooden blocks of 12" in length along the entire surface of the flow-development section. The pattern generally consisted of alternating sets of four and five blocks in one row. A typical velocity profile is presented in Figure 23, where the simulated power-law exponent is $\alpha = 0.33$.

In the lower 20% of the boundary layer height, the flow is then governed by a rough-wall or "law-of-the-wall" logarithmic velocity profile.

$$\frac{U}{u_*} = \frac{1}{\kappa} \ln\left(\frac{z}{z_o}\right)$$

Here, u_* is the surface friction velocity, κ is von Karman's constant, and z_o is the roughness height. This region of the atmospheric boundary layer is relatively unaffected by the Coriolis force, the only region that can be modeled accurately by the wind tunnel (i.e., the lowest 100 m of the atmospheric boundary layer under neutral stability conditions). Thus, it is desirable to have the scaled-model buildings and its surroundings contained within this layer.

The geometric scale of the model should be determined by the size of the wind tunnel, the roughness height, z_o, and the power-law index, α. With a boundary-layer height of 1 m in the test section, the surface layer would be 0.2 m deep for the U.C. Davis ABLWT. For the current study, this boundary layer corresponds to a full-scale height of the order of 800 m. Since the highest elevation of the modeled site investigated in this study is about 160 m full-scale, a majority of the model is contained in this region of full-scale similarity.

Due to scaling effects, full-scale agreement of simulated boundary-layer profiles can only be attained in wind tunnels with long flow-development sections. For full-scale matching of the normalized mean velocity profile, an upwind fetch of approximately 10 to 25 boundary-layer heights can be easily constructed. To fully simulate the normalized turbulence intensity and energy spectra profiles, the flow-development section needs to be extended to about 50 and 100 to 500 times the boundary-layer height, respectively. These profiles must at least meet full-scale similarities in the surface layer region. However, with the addition of spires and other flow tripping devices, the flow development length can be reduced to less than 20 boundary layer heights for most engineering applications.

In the U.C. Davis Atmospheric Boundary Layer Wind Tunnel, the maximum values of turbulence intensity near the surface range from 35% to 40%, similar to that in full scale. Thus, the turbulent intensity profile, u'/u versus z, should agree reasonably with the full-scale, particularly in the region where testing is performed. Figure 24 displays a typical turbulence intensity profile of the boundary layer in the ABLWT test section.

The second boundary-layer condition involves the roughness Reynolds number, Re_z. According to the criterion given by Sutton (1949), Reynolds number independence is attained when the roughness Reynolds number is defined as follows.

$$Re_z = \frac{u_* z_0}{\nu} \geq 2.5$$

Here, u_* is the friction speed, z_0 is the surface roughness length and ν is the kinematic viscosity. Re_z larger than 2.5 ensures that the flow is aerodynamically rough. Therefore, wind tunnels with a high enough roughness Reynolds numbers simulate full-scale aerodynamically rough flows exactly. To generate a rough surface in the wind tunnel, roughness elements are placed on the wind tunnel floor. The height of the elements must be larger than the height of the viscous sub-layer in order to trip the flow. The UC Davis ABLWT satisfies this condition, since the roughness Reynolds number is about 40, when the wind tunnel free stream velocity, $U_{\infty,}$ is equal 3.8 m/s, the friction speed, u_*, is 0.24 m/s, and the roughness height, z_o, is 0.0025 m. Thus, the flow setting satisfies the Re number independence criterion and dynamically simulates the flow.

To simulate the pressure distribution on objects in the atmospheric wind, Jensen (1958) found that the surface roughness to object-height ratio in the wind tunnel must be equal to that of the atmospheric boundary layer, i.e., z_o/H in the wind tunnel must match the full-scale value. Thus, the geometric scaling should be accurately modeled.

The last condition for the boundary layer is the characteristic scale height to boundary layer ratio, H/δ. There are two possibilities for the value of the ratio. If $H/\delta \geq 0.2$, then the ratios must be matched. If $(H/\delta)_{F.S.} < 0.2$, then only the general inequality of $(H/\delta)_{W.T.} < 0.2$ must be met (F.S. stands for full-scale and W.T. stands for wind tunnel). Using the law-of-the-wall logarithmic profile equation, instead of the power-law velocity profile, this principle would constrain the physical model to the 10% to 15% of the wind tunnel boundary layer height.

Along with these conditions, two other constraints have to be met. First, the mean stream wise pressure gradient in the wind tunnel must be zero. Even if high- and low-pressure systems drive atmospheric boundary layer flows, the magnitude of the pressure gradient in the flow direction is negligible compared to the dynamic pressure variation caused by the boundary layer. The other constraint is that the model should not take up more than 5% to 15% of the cross-sectional area at any down wind location. This assures that local flow acceleration affecting the stream wise pressure gradient will not distort the simulation flow.

Simulations in the U.C. Davis ABLWT were not capable of producing stable or unstable boundary layer flows. In fact, proper simulation of unstable boundary layer flows could be a disadvantage in any wind tunnel due to the artificial secondary flows generated by the heating that dominate and distort the longitudinal mean-flow properties, thus, invalidating the similitude criteria. However, this is not considered as a major constraint, since the winds that produce annual an average dispersion are sufficiently strong, such that for flow over a complex terrain, the primary source of turbulence is due to mechanical shear and not due to diurnal or heating and cooling effects in the atmosphere.

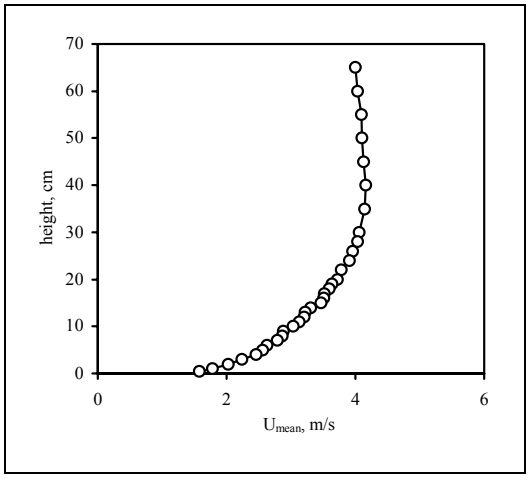

Figure D-1: Mean velocity profile for a typical wind direction in the wind tunnel. The power law exponent α is 0.33. The reference velocity at 65 cm height is 3.55 m/s.

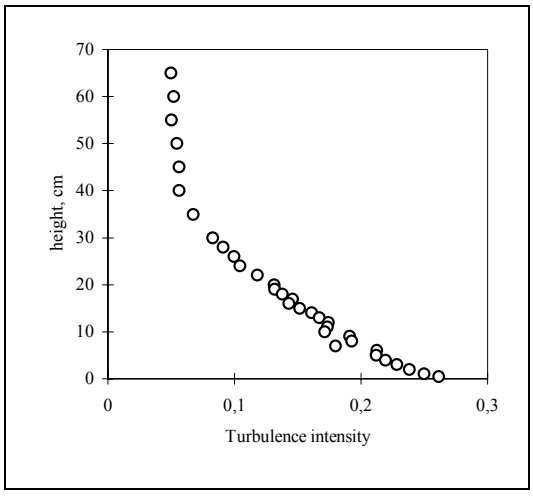

Figure D 2: Turbulence intensity profile for a typical wind direction in the wind tunnel.

APPENDIX F:
WIND-TUNNEL STACK MODELING PARAMETERS

Wind-tunnel simulations use the same fluid, air, as in the full scale. The building Reynolds number, Re, represents a ratio of inertial to viscous forces per unit area and it is often used as a parameter that must be matched between the full scale and the model to insure similarity. Full-scale building Re numbers exceed the tunnel building Re number by several orders of magnitude due to scale reductions, however for the purpose of concentration-profile measurements, flow above a critical building Re number of 11,000 (Snyder, 1981) is essentially Re number independent. The Re number is given by:

$$\mathrm{Re} = \frac{U_H H}{\nu}$$

For lower building Re numbers the critical value for flow independence must be determined experimentally. This was accomplished by repeating tests of ground-level concentration at increased tunnel free-stream velocity and stack flow rate.

Stack emissions in full-scale are turbulent. However, in the wind-tunnel simulations, matching the full-scale stack Re number, Re_s, to that of the model is not possible. In wind- tunnel simulations, adequate similarity is achieved by ensuring that the tunnel stack flow also is turbulent (Snyder, 1981). This condition is generally achieved (for neutral stability conditions) for stack Re number, Re_s, greater than:

$$\mathrm{Re}_s = \frac{U_s D_s}{\nu} > 2300$$

Values as low as 530 may be adequate if trips are used to enhance turbulence. The tunnel stack, for concentration-measurement experiments, has an inside diameter, D_s, of 0.81 cm; for expected stack velocities, U_s, of 12.9 m/s and 2.0 m/s, the stack Re numbers are 6970 and 1080, respectively. The criteria for turbulent stack flow will be achieved if trips are used to enhance the turbulence. For smoke tests the stack inside diameter was exaggerated to 0.25 cm and for a tunnel stack velocity of 5.2 m/s, the stack Re number was 867. The stack again will be tripped to enhance turbulence.

Maintaining a correct ratio of plume momentum to ambient flow requires that (Isyumov and Tanaka, 1980):

$$\frac{\rho_s D_s^2 U_s^2}{\rho_a L^2 U_w^2} = \text{constant}$$

Here, L is a vertical length scale, and U_w is the wind speed at the stack height. For non-buoyant stack exhausts, the stack exhaust density, ρ_s, equals that of the ambient air, ρ_a, and the above relation reduces to:

$$\frac{D_s^2 U_s^2}{L^2 U_w^2} = \text{constant}$$

For a free-stream wind-tunnel air speed of 3.8 m/s, U_w is equal to 2.6 m/s. Thus, for a tunnel stack velocity of 13.7 m/s, satisfaction of the above relation corresponds to a full-scale wind speed at the stack of 5.4 m/s (12 mph) while the full-scale stack velocity, U_s, is 16.3 m/s. For tests with a tunnel stack velocity of 30 m/s, the corresponding full-scale wind speed at the stack outlet is 2.5 m/s (6 mph).

Concentrations measured in the tunnel, C, may be related to full-scale values by the relation

$$\left(\frac{CU_w}{C_s U_s A_s}\right)_{FS} S^2 = \left(\frac{CU_w}{C_s U_s A_s}\right)_{WT}$$

Under similar atmospheric conditions, concentrations measured in the wind tunnel may be related to those in full-scale by this relationship.


ATMOSPHERIC BOUNDARY LAYER WIND TUNNEL